SUPPLEMENTARY INFORMATION

Experimental Section

Protein expression, purification and sample preparation. Yeast GGC (residues 1-300) with C-terminal His-tag (Leu-Glu-His_6) was expressed using a pET-21 vector in *E. coli* BL21(DE3) cells in M9 minimal medium supplemented with 1 g l^{-1} $^{15}NH_4Cl$, 2 g l^{-1} ^{2}H-^{13}C-D-glucose and 98.85% D_2O at 37 °C. Expression was induced by the addition of 0.5 mM isopropyl b-D-thiogalactopyranoside (IPTG) at an OD_{600} of 0.6 and lasted for 4 h. Cells were harvested by centrifugation at 6,000 *g* for 30 min and resuspended in 20 mM HEPES buffer (pH 7.5), 150 mM NaCl, and 5 mM mercaptoethanol (BME). The cells were lysed by sonication in the resuspension buffer containing phenylmethylsulfonyl fluoride (PMSF), followed by pelleting inclusion bodies by centrifugation at 40,000 *g* for 30 min at 4 °C. The GGC-containing inclusion bodies were solubilised in the same buffer with 3 M Guanidinium HCl and 1% of Triton X-100. GGC was purified by Ni-NTA chromatography, and subsequently refolded on column by exchanging the denaturing buffer with buffer containing 3 mM dodecylphosphocholine (DPC) detergent micelles. The refolded protein was then passed through the Superdex-200 (GE healthcare) size exclusion column and eluted as monomers at M.W. ~75 kDa, which is consistent with 34 kDa GGC plus ~40 kDa DPC micelle. Typical NMR sample consists of 0.5 – 1 mM GGC, 50 mM MES (pH 6.0), 2 mM BME, and 80-120 mM DPC.

NMR resonance assignment. NMR spectra were recorded at 30 °C on 600 MHz spectrometer equipped with cryogenic TXI probe (Bruker) using a sample with 0.9 mM *U*-[^{15}N, ^{13}C, ^{2}H]-GGC. Sequence-specific assignment of backbone $^{1}H^{N}$, ^{15}N, $^{13}C^{\alpha}$, $^{13}C^{\beta}$ and $^{13}C'$ chemical shifts was accomplished using the TROSY versions of HNCA, HN(CO)CA, HNCACB, HN(CO)CACB, HN(CA)CO and HNCO.[1] In addition, a 3D (H^{N},H^{N})-HMQC-NOESY-TROSY with ^{15}N, ^{15}N and $^{1}H^{N}$ evolution in the t_1, t_2 and t_3 dimensions, respectively was recorded with the same sample. All spectra were processed using NMRPipe[2] and analysed using CCPNMR.[3]

Structural Characterization of GGC by NMR. Overall, the helical regions determined by RDC-based MFR agree well with ϕ and ψ assigned by TALOS+ based on NMR chemical shift, except for certain regions that contain proline and/or glycine (Figure S3). The carrier proteins have intricate arrangement of helical segments. The fact that the helical segments of GGC agree well with those of AAC and UCP2 is an indication that GGC is folded in DPC micelles and that its overall architecture is similar to that of AAC. The principal structural differences between AAC and GGC are in domain 1: GGC has a longer loop in domain 1 between the C-terminus of H1 and the amphipathic helix *h*1. Moreover, GGC has shorter H1 but longer H6 compared to AAC. The above differences were not revealed by sequence alignment (Figure S4); their characterization required combined analysis using RDC-based MFR and TALOS+.

Substrate titrations. The *U*-[^{15}N, ^{13}C, ^{2}H]-labelled GGC was titrated with 100 mM stock solution of AMP, GDP or GTP solubilised in the NMR buffer. At each substrate concentration point, the $^{1}H^{N}$, ^{15}N, and $^{13}C'$ chemical shift changes induced by substrate binding were measured using the 3D TROSY HNCO spectrum recorded at 30 °C on 600 MHz spectrometer. The combined chemical shift differences ($\Delta\delta_{comb}$) were calculated for each residue using the formula:[4]

$$\Delta\delta^{i}_{comb} = \sqrt{\left(\omega_H \Delta\delta^{i}_{H}\right)^2 + \left(\omega_C \Delta\delta^{i}_{C}\right)^2 + \left(\omega_N \Delta\delta^{i}_{N}\right)^2} \qquad (1)$$

where $\Delta\delta_H$, $\Delta\delta_C$ and $\Delta\delta_N$ are chemical shift perturbations (in ppm) with respect to the ^{1}H, ^{13}C and ^{15}N chemical shift and w_H= 1.00, w_C= 0.34 and w_N= 0.15 are normalization factors. By fitting the $\Delta\delta_{comb}$ vs. [*S*] plot to the classic

equation of binding equilibrium K_D = [*P*][*S*]/[*PS*], where [*P*], [*S*] and [*PS*] represent the concentration of free protein, free substrate and complex, respectively, we determined the apparent dissociation constant (K_D) for each residue. The residue-specific K_D values were determined for GGC both in the presence of GDP and in the presence of GTP (Table S2).

Self-assembly of DNA-origami nanotubes and preparation of aligned samples. For RDC measurements, *U*-[^{15}N, ^{13}C, ^{2}H]-labelled GGC was aligned in 20 mg ml^{-1} DNA-origami nanotubes solution. DNA-origami nanotubes[5] were constructed and purified following the previously published protocol.[6] The buffer of the nanotubes was exchanged into the desired protein buffer by diluting the nanotubes solution twofold with the protein buffer. The nanotubes were then concentrated to 20 mg ml^{-1} using Centricon-100 concentrator units by spinning in 5-min increments at 1,500 *g* and 15 °C. Between 5-min spins, the concentrated solution was mixed slowly by pipetting up and down. The concentration was stopped when the column reached the starting weight. Once the DNA nanotubes were in the appropriate buffer, *U*-[^{15}N, ^{13}C, ^{2}H]-GGC sample was added to reach a final protein concentration of 0.5 mM after concentration using series of 5-min spins at 1,500 *g* and 15 °C. Degree of protein alignment was controlled by measuring residual D_2O quadrupole coupling in the presence of DNA-origami nanotubes.

RDC measurements in liquid crystal formed by DNA-origami nanotubes. We used DNA-origami nanotubes, which can form a stable nematic phase unaffected by detergent,[5] to weakly align GGC for RDC measurements. We optimized the NMR sample buffer such that it is compatible with the use of nanotube alignment medium in the presence and absence of GTP. DNA-origami nanotubes allowed us to measure RDCs of three internuclear vectors, ^{15}N–^{1}H^{N} ($^{1}D_{NH}$), ^{13}C'–^{13}C$^{\alpha}$ ($^{1}D_{C'C\alpha}$) and ^{15}N–^{13}C' ($^{1}D_{NC'}$), in the absence and presence of GTP (Figure S12, Table S3). On average, there are 2.4 and 2.5 RDCs per residue in the absence and presence of GTP, respectively, for regions with confirmed resonance assignment. The two sets of RDCs are, however, quite different considering that the only difference between the two measurements is the addition of GTP. The RDCs were obtained by subtracting *J* of the isotropic sample containing 1 mM GGC in 50 mM MES (pH 6.0), 2 mM BME and 120 mM DPC from *J*+*D* of the aligned sample containing 0.5 mM GGC in the same buffer with added 20 mg ml^{-1} DNA nanotubes[5-6] and 200 mM NaCl. For measuring RDCs for the GTP-bound GGC, 30 mM GTP was added to the aligned sampled by ensuring that the sample pH was not changed. The sign of RDCs follow the convention that $|^{1}J_{NH} + {}^{1}D_{NH}| < 92$ Hz when $^{1}D_{NH}$ is positive. The ^{15}N–^{1}H *J* or *J*+*D* couplings were measured at 600 MHz (^{1}H-frequency) using the *J*-scaled TROSY-HNCO experiment with two interleaved spectra, the regular TROSY-HNCO spectrum and a modified TROSY-HNCO spectrum with J_{NH} evolution during the ^{15}N chemical shift evolution scaled to zero[7]. The ^{15}N –^{13}C' couplings were measured at 600 MHz using the 3D TROSY-HNCO experiment with quantitative $J_{NC'}$ modulations of 33 and 66 ms.[8] The ^{13}C'–^{13}C$^{\alpha}$ couplings were measured at 600 MHz using the 3D TROSY-HNCO experiment with quantitative $J_{C'C\alpha}$ modulations of 0 and 28 ms.[9]

RDC-tensor analysis indicates conformational dynamics. GDO of a given alignment tensor A is defined as |A|/|Amax|, where $|A| = \sqrt{\Sigma A_{ij}^2}$ is the scalar of the order matrix and $|Amax| = \sqrt{2}/3$ is the maximum order; It is a measure of the overall degree of alignment of molecular segments relative to the static magnetic field in solution. For segment with collective motions equal values of GDO are expected. Using GDO as probe for protein internal dynamics was first demonstrated for a relatively rigid protein, ubiquitin.[10] In that study, alignment tensors of one-residue fragments were determined by fitting backbone RDCs (six per residue) to the respective structured fragments in the known X-ray or NMR structure. This approach, however, could not be directly adapted for GGC because 1) there is no high-resolution structure of GGC and 2) RDC data is relatively sparse (< 3 measurements per residue). We instead used RDC-based molecular fragment searching[11] described above to derive GDO for various regions of GGC. We used in this study a fragment size of seven residues; it is a good compromise to correctly fit the tensor parameters with enough couplings and to have enough good hits from the fragment database. In this procedure, RDCs of any given seven-residue segment centred at position *i* were used to search for seven-mer fragments from our fragment library that fit the RDCs with quality factor Q < 25% (Figure S9a).[12] If

the 20 best fragments converge structurally with backbone r.m.s.d. < 0.3 Å, then GDO values of the convergent fragments were calculated based on their respective alignment tensors. The GDO values were then averaged and assigned to the corresponding seven-residue segment of the protein, denoted by ϑ_i, with the uncertainty calculated as below in "*RDC-based Molecular Fragment Analysis*". An example of ϑ_i changing with respect to *i* is illustrated in Figure S9b,c for the H1 helix of GGC in the presence of GTP (Table S4). For this region of GGC, GDO near the N-terminal end of the TM helix is about twice as large as that near the C-terminal end, indicating the presence of significant conformational heterogeneity in domain I of GGC even when the transporter is mostly bound to the substrate. Although the variations in GDO, the Φ/Ψ dihedral angles of the identical amino acids when sliding the MFR-fragment along the sequence are homogenous, as illustrated in Figure S10.

RDC-based Molecular Fragment Analysis. A large fragment library was built that contains 387,751 seven-residue fragments extracted from 858 water-soluble and 934 membrane-associated protein crystal structures (resolution < 2.5 Å). The RDCs of every possible seven-residue sequence of the protein were fitted to all the fragments of the library by singular value decomposition (SVD) using the program PALES.[13] Only those seven-residue stretches with more than 8 RDCs were used for fragment searching. In the end, only fragments with Q_{free} < 25% were collected. We used the 20-best fitting fragments converging structurally with a backbone r.m.s.d. < 0.3 Å. We determined the General Degree of Order (GDO) as defined in reference [10] that characterizes the magnitude of alignment for a given seven-residue segment centred at position *i* using the formula below:

$$GDO_i = \vartheta_i = \sqrt{\frac{2}{3}\sum_{ij} S_{ij}^2} = \sqrt{S_{zz}^2\left(1+\frac{\eta^2}{3}\right)} = |A_a|\sqrt{1+\left(3/4\,Rh^2\right)} \qquad (2)$$

where A_a is the degree of alignment and *Rh* is the rhombicity of the alignment tensor. A_a and *Rh* were directly extracted by the program PALES from the SVD fit. Given the errors in RDC measurements, the uncertainties of the alignment tensor elements were obtained during the SVD fit using a 1000 Monte-Carlo steps simulation[13] (implemented in the program PALES). For each of the 20 best fragments, the uncertainty in GDO was calculated based on the uncertainties of the alignment tensor elements. Finally, the GDO uncertainty due to errors in RDC measurements (ΔGDO_{rdc}) is the average of the GDO uncertainties of the 20 fragments. In addition, the GDO uncertainty due to errors from structural diversity of the 20 fragments (ΔGDO_{frag}) is the standard deviation of the 20 GDO values. The final GDO uncertainty $\Delta GDO = (\Delta GDO_{rdc}^2 + \Delta GDO_{frag}^2)^{1/2}$. To map local conformational variability of the protein, we determined the derivative of GDO ($\Delta\vartheta_i = |\vartheta_i - \vartheta_{i+3}|$), between neighbouring segments separated by three residues.

References

[1] a) M. Salzmann, G. Wider, K. Pervushin, H. Senn, K. Wuthrich, *J. Am. Chem. Soc.* **1999**, *121*, 844-848; b) L. E. Kay, M. Ikura, R. Tschudin, A. Bax, *J. Magn. Reson.* **1990**, *213*, 423-441.

[2] F. Delaglio, S. Grzesiek, G. W. Vuister, G. Zhu, J. Pfeifer, A. Bax, *J. Biomol. NMR* **1995**, *6*, 277-293.

[3] W. F. Vranken, W. Boucher, T. J. Stevens, R. H. Fogh, A. Pajon, M. Llinas, E. L. Ulrich, J. L. Markley, J. Ionides, E. D. Laue, *Proteins* **2005**, *59*, 687-696.

[4] F. H. Schumann, H. Riepl, T. Maurer, W. Gronwald, K. P. Neidig, H. R. Kalbitzer, *J. Biomol. NMR* **2007**, *39*, 275-289.

[5] S. M. Douglas, J. J. Chou, W. M. Shih, *Proc. Natl. Acad. Sci. USA* **2007**, *104*, 6644-6648.

[6] G. Bellot, M. A. McClintock, J. J. Chou, W. M. Shih, *Nat. Protoc.* **2013**, *8*, 755-770.

[7] G. Kontaxis, G. Clore, A. Bax, *J. Magn. Reson.* **2000**, *143*, 184-196.

[8] J. J. Chou, F. Delaglio, A. Bax, *J. Biomol. NMR* **2000**, *18*, 101-105.

[9] C. P. Jaroniec, T. S. Ulmer, A. Bax, *J. Biomol. NMR* **2004**, *30*, 181-194.

[10] J. R. Tolman, H. M. Al-Hashimi, L. E. Kay, J. H. Prestegard, *J. Am. Chem. Soc.* **2001**, *123*, 1416-1424.

[11] a) F. Delaglio, G. Kontaxis, A. Bax, *J. Am. Chem. Soc.* **2000**, *122*, 2142-2143; b) M. J. Berardi, W. M. Shih, S. C. Harrison, J. J. Chou, *Nature* **2011**, *476*, 109-113.
[12] G. Cornilescu, J. L. Marquardt, M. Ottiger, A. Bax, *J. Am. Chem. Soc.* **1998**, *120*, 6836-6837.
[13] M. Zweckstetter, *Nat. Protoc.* **2008**, *3*, 679-690.
[14] R. Sanchez, A. Sali, *Methods Mol. Biol.* **2000**, *143*, 97-129.
[15] A. J. Robinson, E. R. Kunji, *Proc. Natl. Acad. Sci. USA* **2006**, *103*, 2617-2622.

SUPPLEMENTARY FIGURES

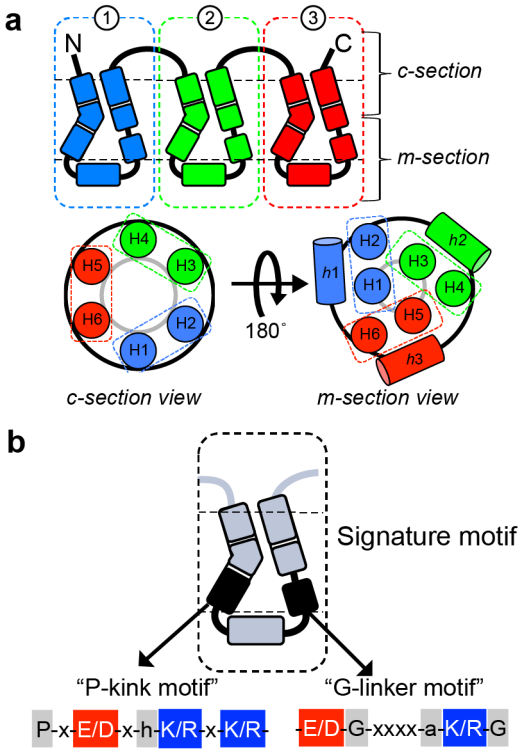

Figure S1. Schematic diagram of the carrier tripartite structure. (a) The three pseudo repeats are colour-coded in blue, green and red, respectively. Each repeat contains two TM helices separated by an amphipathic helix. The cytoplasmic and matrix views are shown. (b) The signature sequence motifs, the proline-kink (P-kink) motif and the glycine-rich linker (G-linker) motif, are highlighted in black.

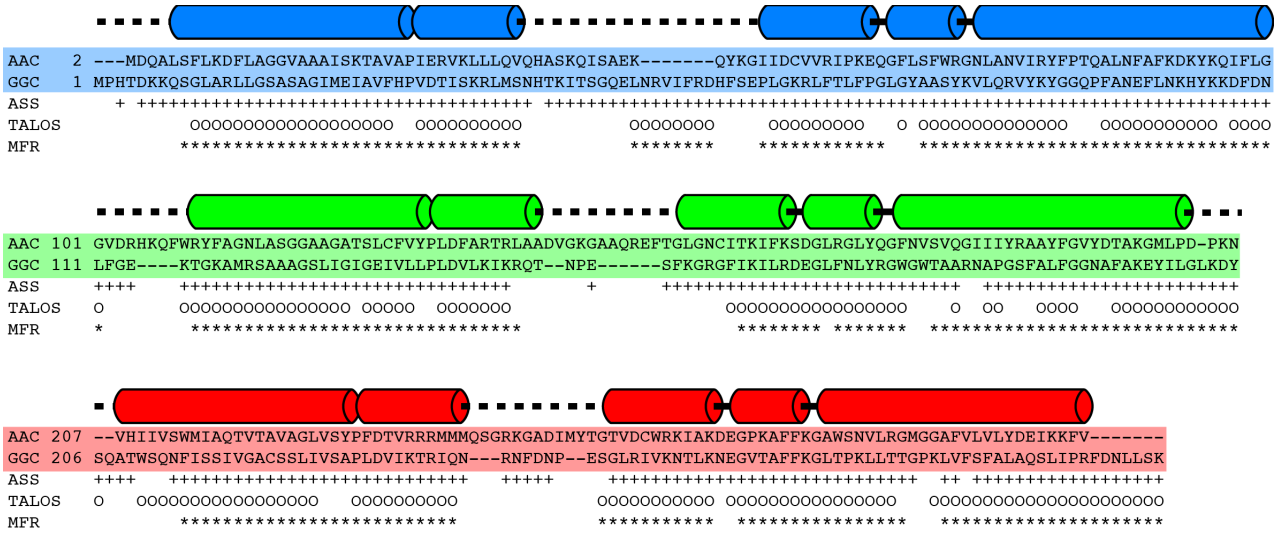

Figure S2. Structural alignment of AAC and GGC. AAC and GGC sequences aligned based on the secondary structures and sequence motifs. Helical regions of the AAC crystal structure are shown as cylinders, which are colour-coded in blue, green or red for each of the three pseudo repeats. GGC residues of which NMR resonances have been assigned are indicated with a cross. Residues predicted by TALOS+ or RDC-based MFR to be helical are indicated with a circle or star, respectively.

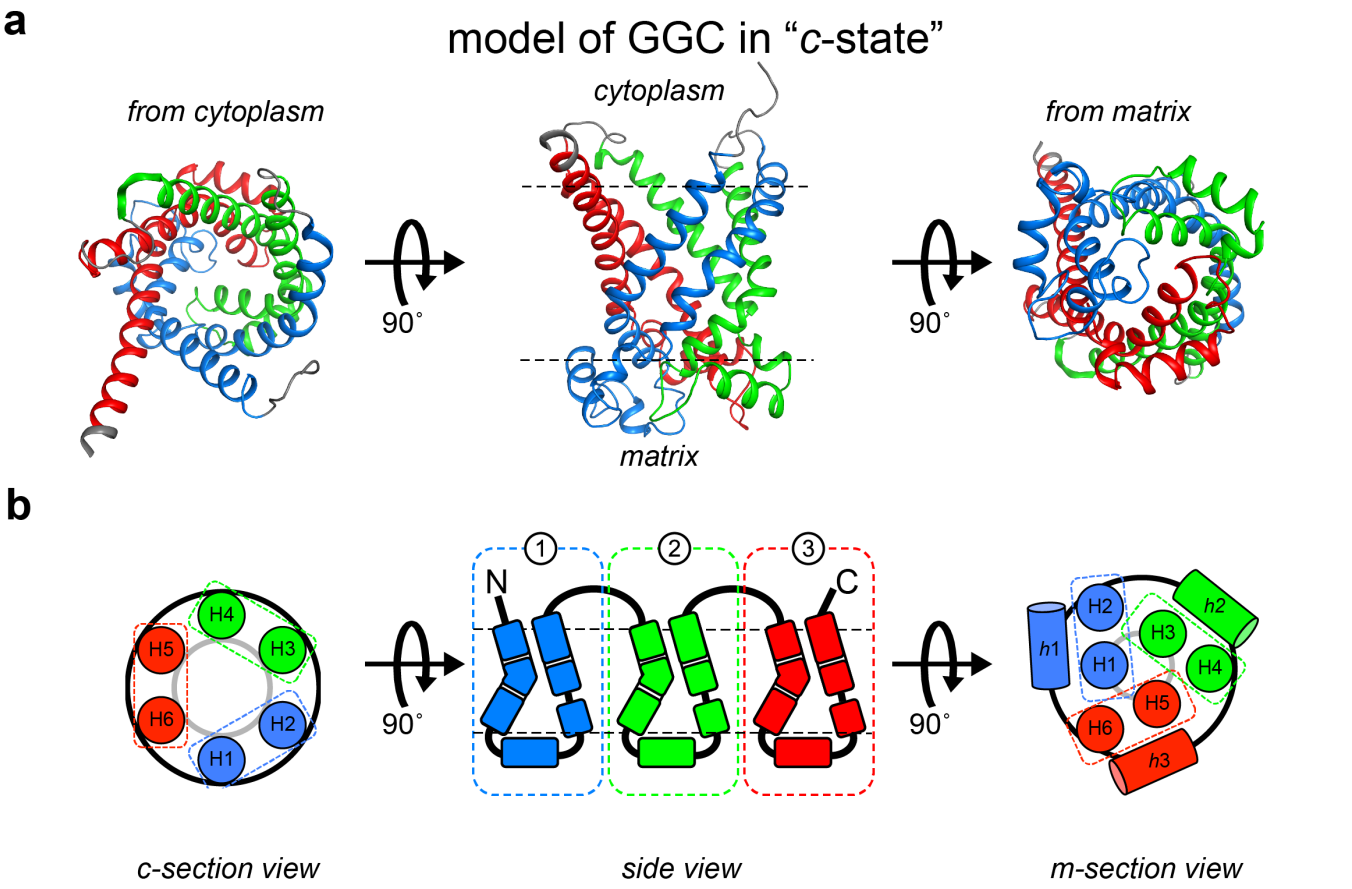

Figure S3. Structural model of GGC. a) Ribbon representation of the GGC model built based on the crystal structure of the inhibited state of AAC (PDB code: 1okc) and the sequence alignment in b. The GGC model was obtained using the program Modeller.[14] The three views are: view from the cytoplasm side (left), view from within the membrane (middle), and view from the matrix side (right). B) Schematic representation of the different view shown in a).

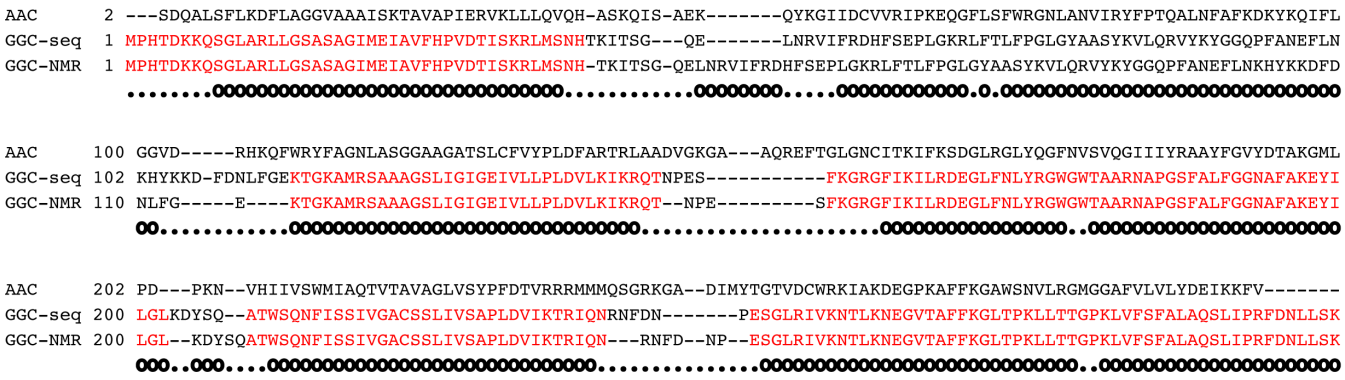

Figure S4. Double sequence alignment between AAC and GGC. The sequence GGC-seq was aligned to the bovine AAC sequence using symmetry-related triplets proposed by Robinson et al. GGC-NMR sequence was aligned using NMR experimental data. Helical secondary structures determine by NMR is indicated by black circle. The red characters show when GGC-seq and GGC-NMR sequences are aligned.

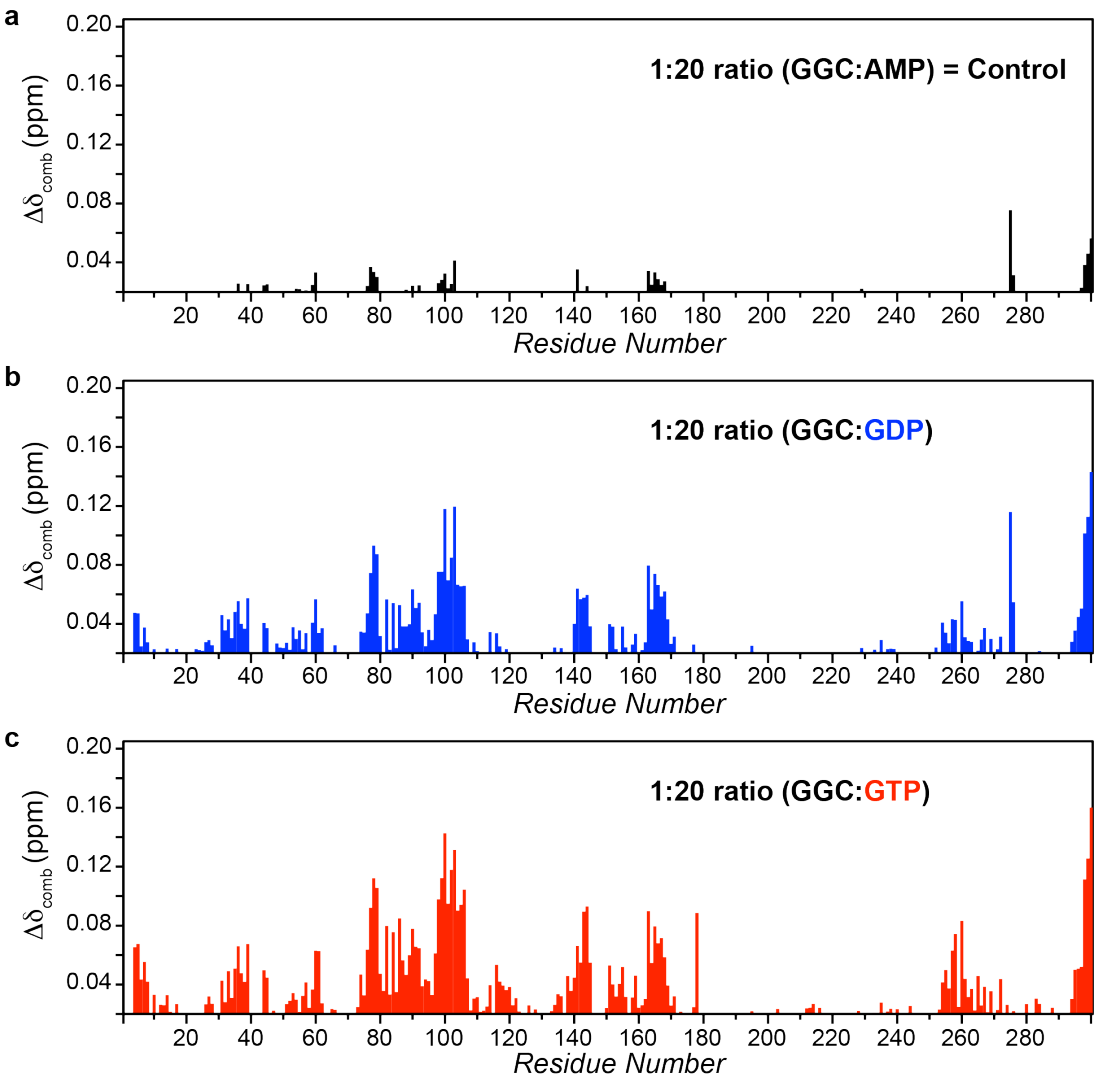

Figure S5. Chemical shift perturbation of GGC by mono-, di-, and tri-phosphate nucleotides. Bar plots showing the combined chemical shift changes (defined in Methods) induced by the addition of 20-fold molar excess of a) AMP (black bar), b) GDP (blue bar) and c) GTP (red bar).

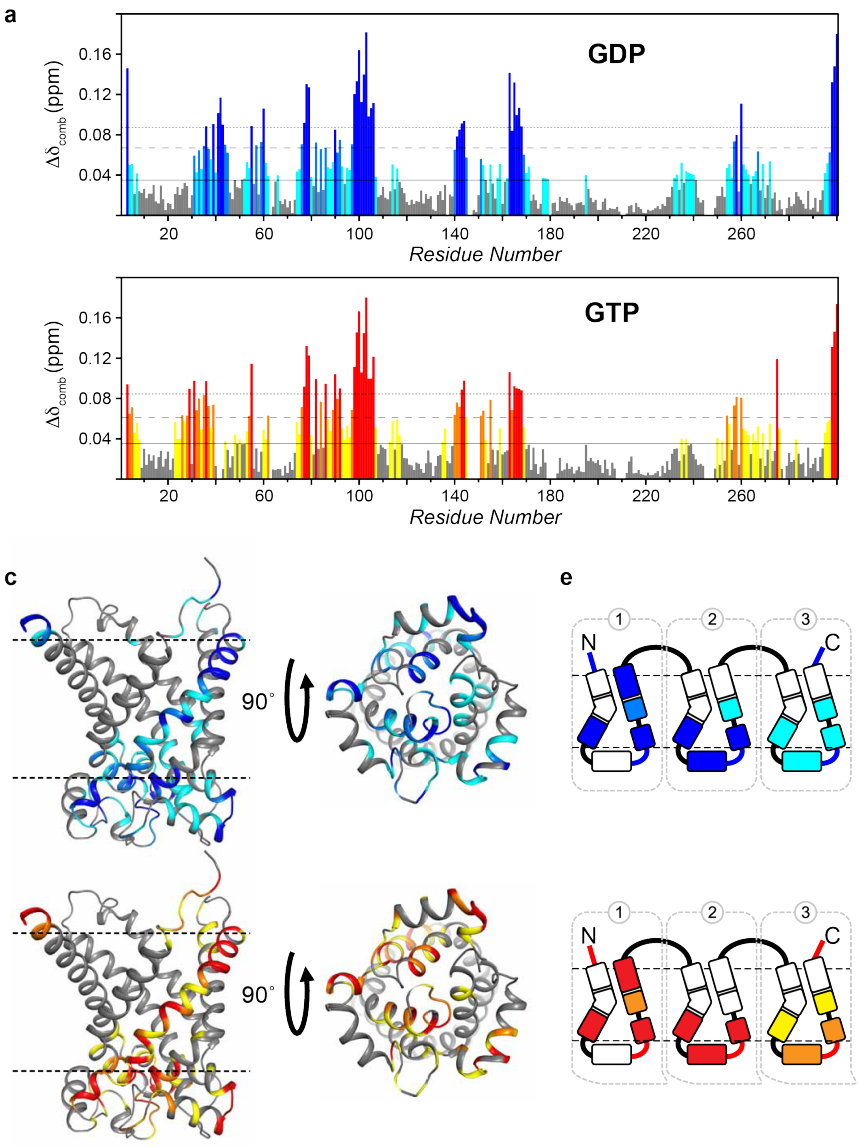

Figure S6. Chemical shift perturbation analysis of GDP and GTP binding to GGC. Residue-specific chemical shift changes induced by a) 60 mM GDP and b) 30 mM GTP. The residues are categorized into the following groups: gray – less than mean (indicated by the black horizontal line); cyan for GDP or yellow for GTP – mean to mean + 1 *s.d.* (indicated by the dashed line); marine for GDP or orange for GTP – mean + 1 *s.d.* to mean + 2 *s.d.* (indicated by the dotted line); and blue for GDP or red for GTP – greater than or equal to mean + 2 *s.d.*. c) d) Mapping of chemical shift perturbation onto the GGC model for GDP and GTP binding. Views from the membrane and matrix sides are shown in the left and right panels, respectively. e) (f) Mapping of chemical shift perturbation onto the carrier tripartite drawing as in c and d.

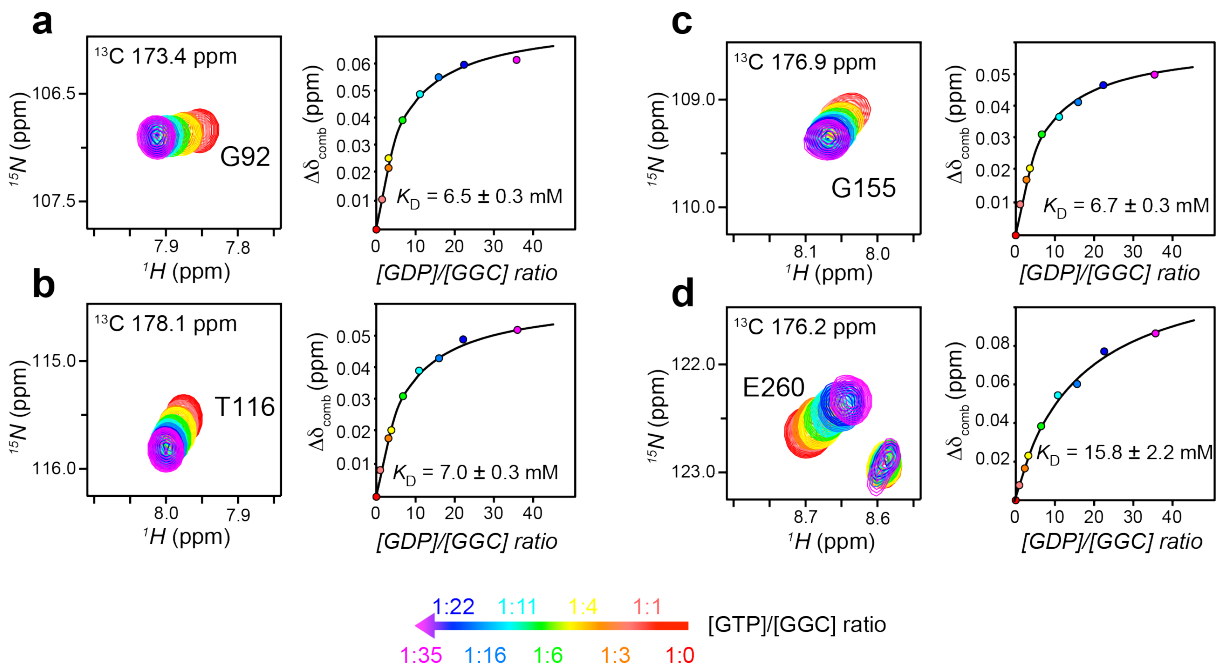

Figure S7. Residue-specific K_D of GGC–GTP binding. Samples of chemical shift perturbation from 3D TROSY HNCO spectra of GGC for residues G82 (a), T116 (b), G155 (c), E260 (d) upon incremental addition of GTP. The NMR peaks at different substrate/protein molar ratio are shown with the linear color spectrum scale from ratio = 0 (red) to ratio = 35 for GDP (magenta). For each of the perturbed resonances, the chemical shift changes (defined in Methods) vs. GTP/GGC molar ratio are plotted and fitted to the standard equation of binding equilibrium (right panels).

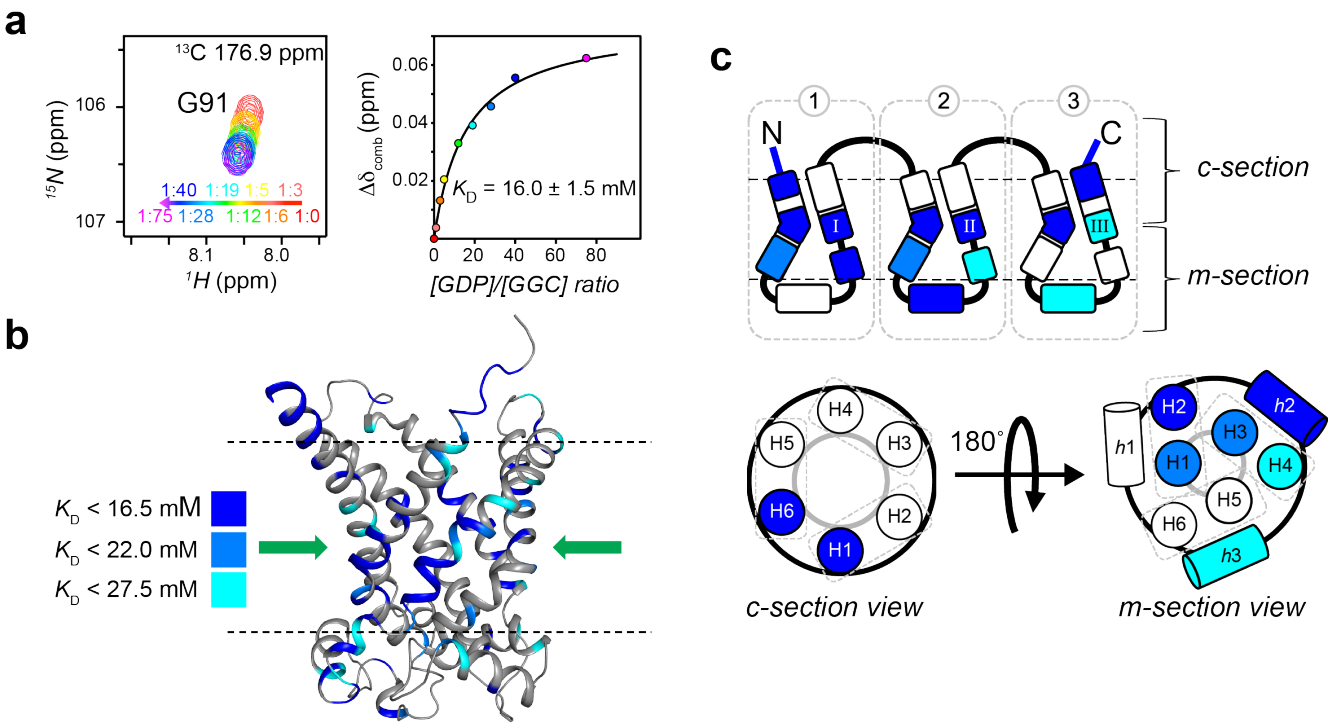

Figure S8. Residue-specific K_D of GGC–GDP binding. a) Sample chemical shift perturbation from 3D TROSY HNCO spectra of GGC upon incremental addition of GDP. The NMR peaks at different substrate/protein molar ratio are shown with the linear color spectrum scale from ratio = 0 (red) to ratio = 75 for GDP (magenta). For each of the perturbed resonances, the chemical shift changes (defined in Methods) vs. GDP/GGC molar ratio are plotted and fitted to the standard equation of binding equilibrium (right panels). b) Mapping residue-specific K_D onto the GGC model for GDP binding with color-code defined in the figure. The common binding site (CBS) of nucleotide carrier proteins as proposed based on conservation of amino acid, comparative model and chemical properties,[15] is indicated by the green arrow. c) The K_D values in b are shown in the context of the schematic diagram of the tripartite topology and of the cytoplasmic and matrix views for providing a conceptual view of nucleotide binding.

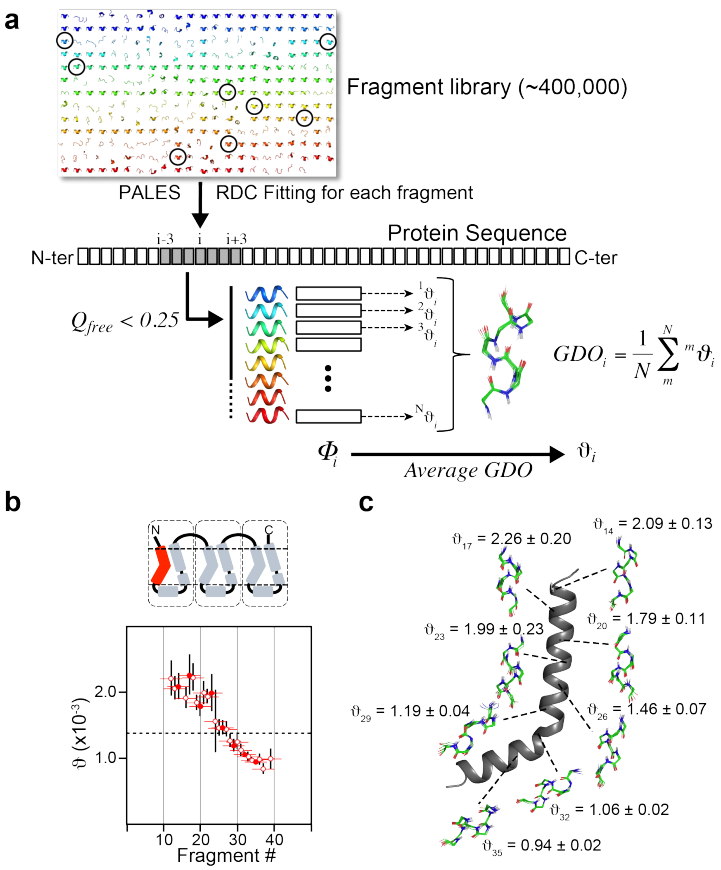

Figure S9. Computing Generalized Degree of Order (GDO) using RDCs. (a) Schematic illustration of the method for deriving fragment-specific GDO by RDC-based molecular fragment searching. For each seven-residue sequence (i-3 – i+3) of the protein with greater than 8 RDCs, the seven-residue fragments from the fragment library that fit to the RDCs with Q < 25% are collected and sorted by increasing Q. If the top 20 fragments converge structurally (backbone r.m.s.d. < 0.3Å), then the average GDO is calculated for the fragment ensemble and assigned as the GDO of the seven-residue sequence centred at i with the standard deviation determined by Monte-Carlo simulation for each fragment. (b) A plot of GDO values vs. sliding seven-residue fragments for the H1 helix of GTP-bound GGC, showing significant GDO variation within the TM helix. The red horizontal lines represent the sizes of the fragments, and the vertical lines are the uncertainties in GDO calculation as described in a. (c) Examples of fragment ensembles (lines) and their corresponding GDO values from the H1 helix (gray ribbon) of the GTP-bound GGC as in b. The GDO values are multiplied by 1,000 for convenience.

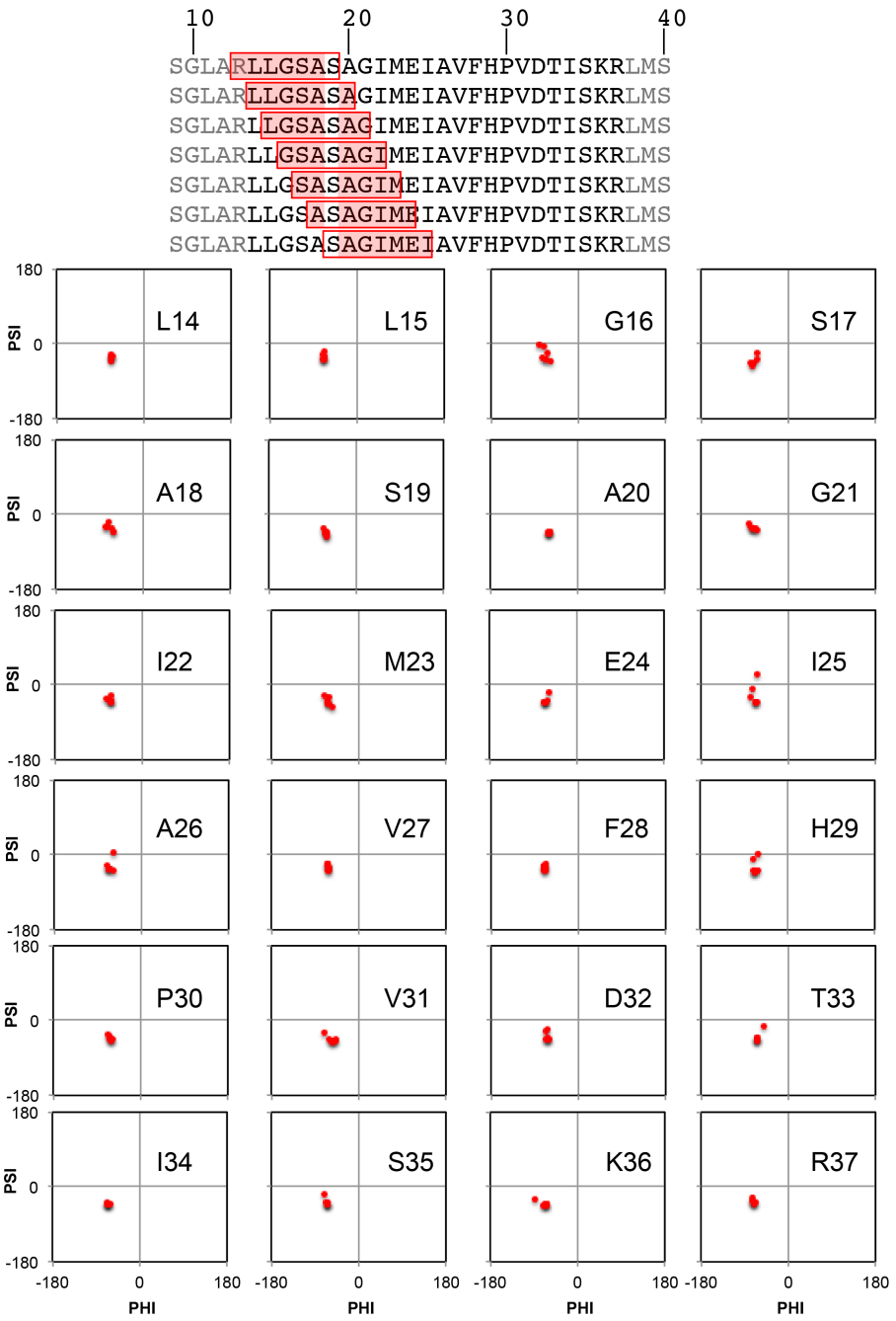

Figure S10. Correlation of backbone Φ/Ψ dihedral angles of the same residue from sliding fragments. Top panel shows an example of sliding fragments for residue S19. Lower panel shows the Ramachadran plots for residues in the H1 helix.

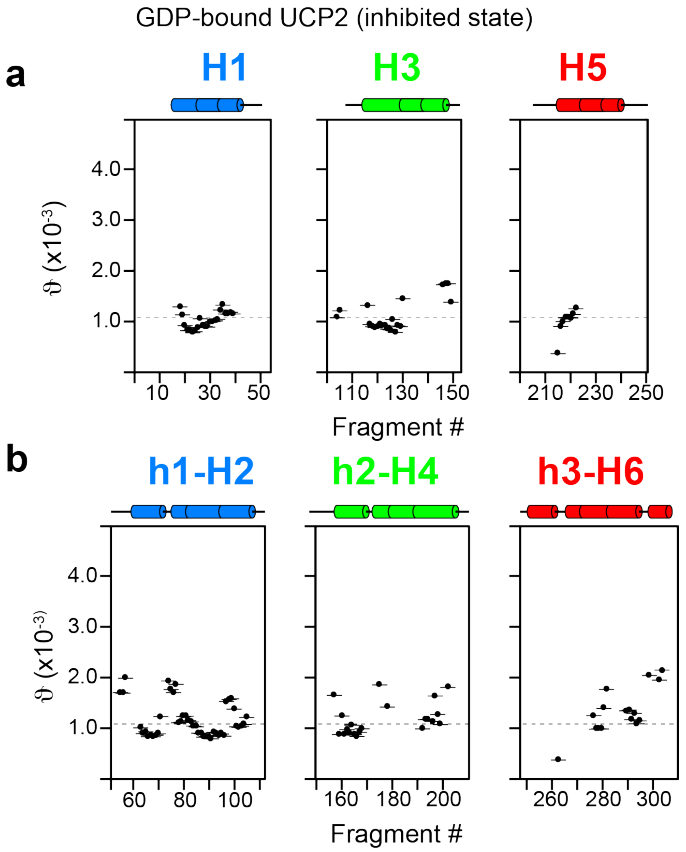

Figure S11. Mapping Conformational heterogeneity in UCP2. Mapping conformational heterogeneity for inhibited state of UCP2. GDO variation as shown by the plot of GDO values vs. sliding seven-residue fragments for (a) H1, H3 and H5 and (b) H2, H4 and H6.

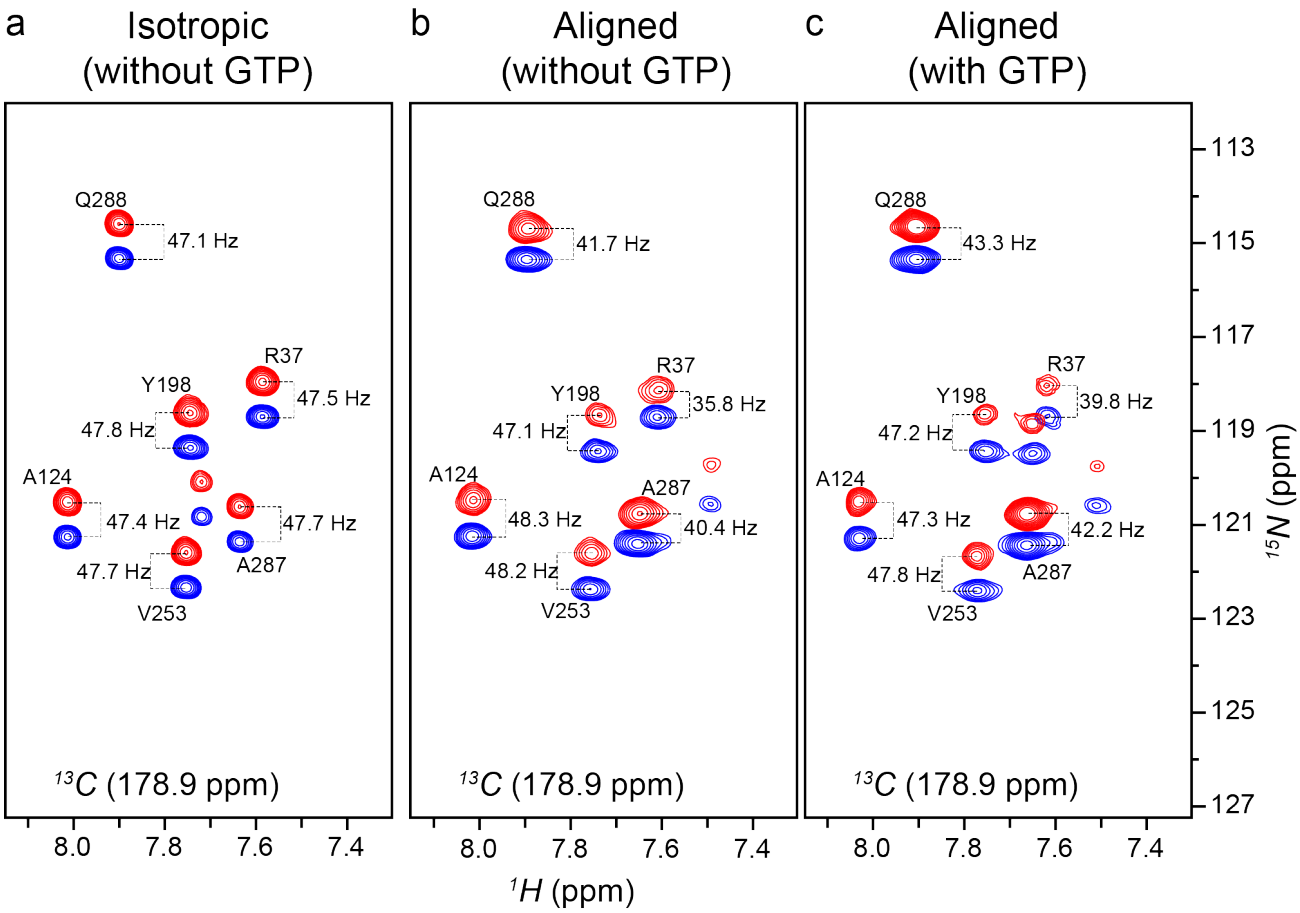

Figure S12. Measurement of $^1D_{NH}$ RDCs of GGC weakly aligned in the DNA-origami nanotube liquid crystal. Shown here are sample regions of the 3D *J*-scaled TROSY-HNCO spectra recorded using a) the isotropic sample in the absence of substrate, b) the aligned sample in the absence of substrate, and c) the aligned sample in the presence of 30 mM GTP at ^{1}H frequency of 600 MHz. For each of the samples above, two inter-leaved spectra were recorded, the regular TROSY-HNCO (blue peaks) and a modified TROSY-HNCO with J_{NH} evolution during the ^{15}N chemical shift evolution scaled to zero (red peaks). The difference in ^{15}N frequency between the red and black peaks is $^1J_{NH}/2$ for the isotropic sample and $(^1J_{NH}+^1D_{NH})/2$ for the aligned samples. $^1D_{NH}$ was determined from the two values.

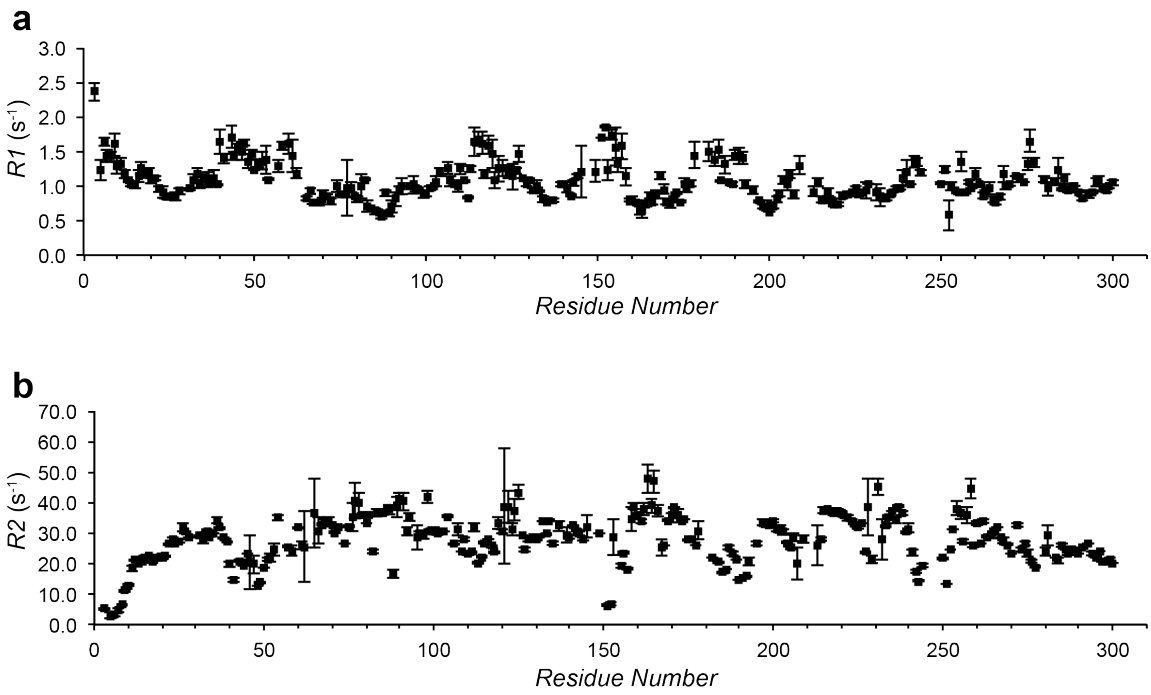

Figure S13. **^{15}N NMR Relaxation measurements.** The residue-specific ^{15}N R1 (a) and R2 (b) of GGC in the absence of substrate measured at 800 MHz.

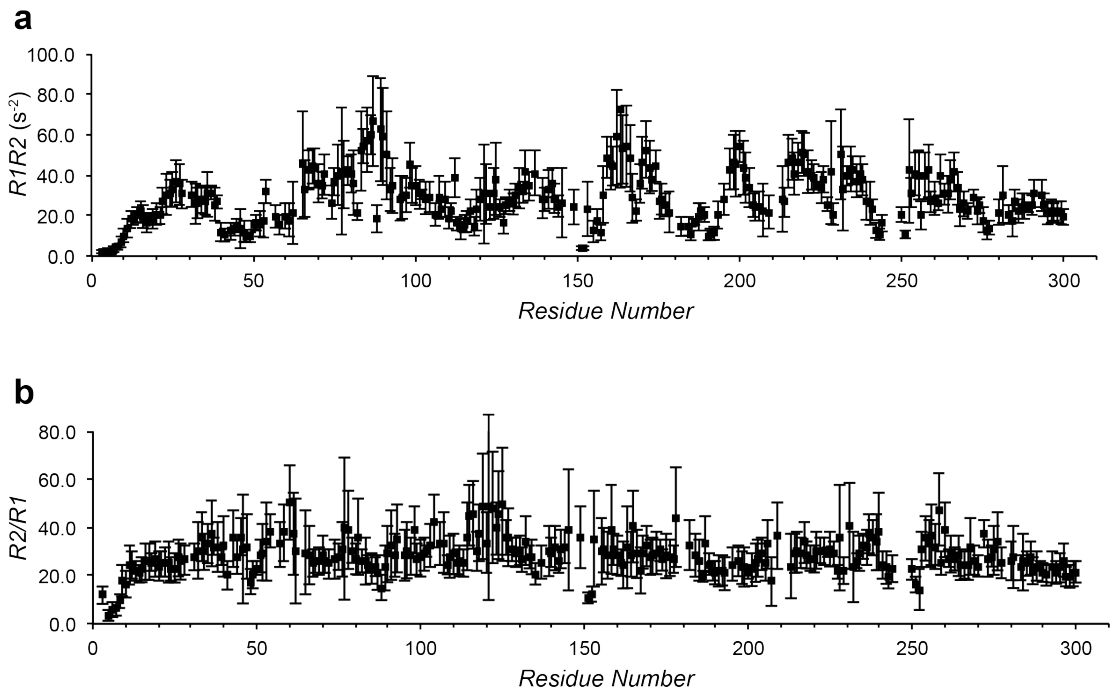

Figure S14. Product and ratio of ^{15}N NMR relaxation measurements. The product of ^{15}N R1 and R2 for probing variations in chemical exchange (a) and the ratio of ^{15}N R2 to R1 for probing variations in the correlation times (b). The relaxation rates are from Figure S13 above.

SUPPLEMENTARY TABLES

Table S1. Backbone Carbon Chemical Shift of *U*-[^{2}H, ^{15}N, ^{13}C]-GGC in DPC micelles

#	Residue	$C\alpha$ (ppm)	$C\beta$ *(ppm)*	*C' (ppm)*
1	MET			
2	PRO	55.5	29.3	173.8
3	HIS	56.8	29.6	178.9
4	THR	61.2	69.3	173.9
5	ASP	53.9	40.9	176.2
6	LYS	56.0	31.9	176.7
7	LYS	56.1	31.9	176.7
8	GLN	55.3	29.4	175.9
9	SER	57.7	63.9	175.2
10	GLY	46.3		175.7
11	LEU	57.3	41.0	178.1
12	ALA	54.8	17.4	180.6
13	ARG	58.2	29.1	178.7
14	LEU	57.3	41.3	178.3
15	LEU	56.7	40.8	179.1
16	GLY	46.3		176.1
17	SER	60.4	62.8	175.8
18	ALA	53.8	18.0	178.2
19	SER	60.5	62.7	175.5
20	ALA	54.0	17.8	179.8
21	GLY	46.2		175.5
22	ILE	63.2	37.0	176.9
23	MET	56.8	30.9	177.9
24	GLU	57.5	28.9	177.8
25	ILE	62.3	37.5	176.6
26	ALA	53.5	18.2	178.0
27	VAL	62.6	31.3	175.8
28	PHE	57.5	38.8	175.1
29	HIS	54.7	28.3	173.1
30	PRO	64.4	31.3	177.9
31	VAL	65.2	30.6	177.8
32	ASP	56.6	40.8	177.9
33	THR	65.4	68.4	176.5
34	ILE	64.2	37.0	177.4
35	SER	61.8	62.2	176.3
36	LYS	58.6	31.6	178.9
37	ARG	57.2	29.4	178.1
38	LEU	56.1	41.6	177.7
39	MET	55.8	32.0	177.0
40	SER	58.8	63.1	174.6
41	ASN	53.3	31.4	175.3
42	HIS	57.7	29.4	175.2
43	THR	62.2	69.2	174.4
44	LYS	56.1	32.1	176.5

45	ILE	61.0	37.7	176.3
46	THR	61.3	69.2	174.5
47	SER	58.3	63.6	175.2
48	GLY	45.6		174.6
49	GLN	56.3	28.6	176.8
50	GLU	57.0	29.1	177.3
51	LEU	55.9	41.0	177.3
52	ASN	54.2	38.4	175.8
53	ARG	57.2	29.7	177.0
54	VAL	63.6	31.5	176.4
55	ILE	62.0	37.4	176.3
56	PHE	58.4	38.5	176.1
57	ARG	56.8	29.8	176.5
58	ASP	54.8	40.5	176.6
59	HIS	56.1	29.6	174.7
60	PHE	57.8	38.9	175.4
61	SER	58.9	63.1	174.5
62	GLU	56.5	38.8	175.0
63	PRO	66.0	30.6	177.6
64	LEU	57.4	41.1	178.6
65	GLY	47.0		175.0
66	LYS	58.6	31.7	179.2
67	ARG	58.1	29.3	178.8
68	LEU	57.7	40.9	178.0
69	PHE	59.5	37.8	177.3
70	THR	64.3	68.6	175.5
71	LEU	56.3	42.0	176.5
72	PHE	54.9	38.6	173.1
73	PRO	64.1	30.8	178.5
74	GLY	45.2		174.9
75	LEU	55.9	41.5	176.6
76	GLY	45.0		174.8
77	TYR	60.4	37.6	177.1
78	ALA	54.5	17.5	179.4
79	ALA	53.6	17.9	179.2
80	SER	60.9	63.0	175.5
81	TYR	60.6	37.4	177.1
82	LYS	58.7	31.2	179.7
83	VAL	66.1	30.8	177.6
84	LEU	57.4	40.2	178.4
85	GLN	59.0	28.3	178.5
86	ARG	58.6	29.2	178.7
87	VAL	65.6	30.8	177.3
88	TYR	60.6	38.1	177.2
89	LYS	58.0	31.5	178.3
90	TYR	59.3	38.0	176.9
91	GLY	45.6		173.4
92	GLY	45.3		174.1
93	GLN	56.0	37.3	174.8
94	PRO	64.8	30.6	178.0
95	PHE	59.1	38.3	176.6
96	ALA	53.9	18.1	178.4
97	ASN	55.4	38.5	176.9

98	GLU	58.3	28.7	177.9
99	PHE	60.7	38.9	177.4
100	LEU	56.8	40.8	178.2
101	ASN	54.9	38.4	176.6
102	LYS	57.3	31.8	177.4
103	HIS	56.7	29.7	175.1
104	TYR	58.6	38.4	175.6
105	LYS	57.4	31.8	176.8
106	LYS	57.1	31.6	177.0
107	ASP	55.2	40.6	177.2
108	PHE	59.5	38.5	176.6
109	ASP	56.1	39.9	177.9
110	ASN	54.0	38.3	176.2
111	LEU	56.6	41.6	176.8
112	PHE	57.1	39.1	176.3
113	GLY	44.9		174.5
114	GLU	57.5	29.5	177.8
115	LYS	57.4	31.7	178.0
116	THR	63.6	68.5	175.9
117	GLY	46.3		175.2
118	LYS	57.8	31.9	178.0
119	ALA	53.5	18.0	179.3
120	MET	57.0	32.1	177.1
121	ARG	57.8	29.6	177.7
122	SER	59.5	62.9	175.8
123	ALA	53.3	18.0	178.7
124	ALA	53.1	18.3	178.0
125	ALA	53.3	18.2	178.8
126	GLY	45.6		175.0
127	SER	59.2	63.2	174.8
128	LEU	55.8	41.2	177.4
129	ILE	62.1	37.4	176.8
130	GLY	45.6		175.6
131	ILE	62.5	37.3	177.0
132	GLY	46.2		174.5
133	GLU	57.5	29.3	177.6
134	ILE	62.4	37.5	176.4
135	VAL	62.8	31.4	175.0
136	LEU	54.8	41.0	177.6
137	LEU	54.3		175.7
138	PRO	63.6	30.1	176.9
139	LEU	56.1	40.8	177.9
140	ASP	55.6	40.1	178.0
141	VAL	64.0	31.2	176.8
142	LEU	55.8	40.8	177.3
143	LYS	57.1	31.3	177.2
144	ILE	61.8	37.4	176.8
145	LYS	56.4	32.0	176.8
146	ARG			
147	GLN			
148	THR	61.6	69.4	174.0
149	ASN	51.1	38.5	173.5
150	PRO	63.5	31.3	177.4

151	GLU	56.7	29.1	177.1
152	SER	58.6	63.2	174.5
153	PHE	57.6	38.6	175.8
154	LYS	56.4	32.0	176.9
155	GLY	45.4		174.3
156	ARG	56.7	30.0	177.2
157	GLY	45.6		175.0
158	PHE	60.2	38.7	176.7
159	ILE	63.4	35.7	177.1
160	LYS	58.8	31.4	178.1
161	ILE	64.2	37.0	177.8
162	LEU	57.2	40.8	178.4
163	ARG	58.0	29.6	178.3
164	ASP	56.0	40.4	177.9
165	GLU	56.7	29.2	177.6
166	GLY	45.6		175.2
167	LEU	57.2	41.2	177.9
168	PHE	59.6	37.3	177.2
169	ASN	54.9	37.7	177.4
170	LEU	56.9	41.2	177.8
171	TYR	59.3	37.8	176.6
172	ARG	57.4	29.3	177.6
173	GLY	45.3		174.5
174	TRP	57.6	29.0	176.7
175	GLY	45.7		174.2
176	TRP	58.0	29.0	176.8
177	THR	62.8	68.8	174.8
178	ALA	52.8	18.1	178.0
179	ALA		18.3	178.0
180	ARG			
181	ASN	52.7	38.8	174.5
182	ALA	51.0	17.3	175.3
183	PRO	63.4	31.0	177.5
184	GLY	45.2		174.6
185	SER	58.9	63.2	174.7
186	PHE	58.2	38.4	175.8
187	ALA	52.7	18.3	178.0
188	LEU	55.9	41.5	177.0
189	PHE	57.3	38.4	176.2
190	GLY	45.4		174.7
191	GLY	45.2		174.1
192	ASN	53.6	38.7	175.3
193	ALA	53.6	18.2	178.4
194	PHE	58.9	38.4	176.4
195	ALA	53.7	18.1	178.5
196	LYS	59.3	31.6	177.6
197	GLU	58.7	28.6	178.9
198	TYR	60.4	38.0	177.5
199	ILE	63.2	36.7	177.5
200	LEU	56.8	40.2	179.2
201	GLY	45.8		175.4
202	LEU	56.1	41.0	178.1
203	LYS	58.1	31.7	177.2

204	ASP	55.2	40.2	177.4
205	TYR	59.1	37.7	176.8
206	SER	59.6	63.1	174.7
207	GLN	55.8	28.4	176.1
208	ALA	52.3	18.4	178.0
209	THR	62.6	69.0	175.2
210	TRP			
211	SER			
212	GLN	57.9	27.9	177.8
213	ASN	54.9	37.8	177.1
214	PHE	60.7	38.6	177.3
215	ILE	64.1	36.3	177.9
216	SER	61.7	62.0	177.8
217	SER	61.5	62.3	176.4
218	ILE	64.1	36.7	177.8
219	VAL	66.6	30.7	179.0
220	GLY	46.6		176.3
221	ALA	54.2	17.9	179.8
222	CYS	62.5	27.1	176.3
223	SER	61.4	62.4	175.8
224	SER	60.3	62.7	175.8
225	LEU	56.4	41.7	177.8
226	ILE	62.4	37.3	176.3
227	VAL	62.6	31.4	176.4
228	SER	58.5	63.4	173.8
229	ALA	50.7	17.7	175.6
230	PRO	63.1	30.0	177.4
231	LEU	57.2	40.6	178.3
232	ASP	56.9	39.8	178.7
233	VAL	65.0	31.2	178.1
234	ILE	64.4	37.1	177.3
235	LYS	59.8	31.6	178.4
236	THR	65.3	68.5	176.1
237	ARG	57.4	29.2	178.2
238	ILE	63.1	37.3	177.1
239	GLN	57.2	28.5	176.6
240	ASN	53.2	38.2	175.2
241	ARG	55.9	29.2	175.4
242	ASN	52.9	38.5	174.9
243	PHE	57.2	38.8	175.2
244	ASP	54.0	40.8	175.5
245	ASN	51.2	36.4	173.7
246	PRO			
247	GLU			
248	SER			
249	GLY	46.3		174.8
250	LEU	56.7	40.8	178.2
251	ARG	58.6	29.1	177.9
252	ILE	63.4	37.0	178.8
253	VAL	65.7	30.9	177.2
254	LYS	59.4	31.5	178.0
255	ASN	54.9	37.5	177.4
256	THR	65.6	68.3	175.6

257	LEU	56.4	40.7	177.1
258	LYS	56.7	31.8	176.9
259	ASN	54.0	39.0	176.1
260	GLU	57.7	29.4	177.8
261	GLY	45.6		175.4
262	VAL	65.4	31.2	177.6
263	THR	66.2	67.6	176.8
264	ALA	54.5	17.7	180.2
265	PHE	60.3	38.4	177.1
266	PHE	60.4	38.5	177.7
267	LYS	58.8	31.4	178.4
268	GLY	45.2		174.7
269	LEU	55.2	41.9	177.2
270	THR	64.4	67.8	173.6
271	PRO	64.8	30.7	178.4
272	LYS	57.3	31.4	178.3
273	LEU	56.5	41.4	177.6
274	LEU	55.7	41.1	177.5
275	THR	62.4	69.1	175.4
276	THR	62.8	69.1	175.1
277	GLY	46.1		172.2
278	PRO			
279	LYS	57.2	31.6	177.6
280	LEU	55.8	41.3	177.4
281	VAL	63.4	29.3	176.2
282	PHE	58.6	38.5	175.5
283	SER	58.7	63.7	175.0
284	PHE	59.7	38.2	176.7
285	ALA	54.3	17.4	180.1
286	LEU	56.7	41.0	179.0
287	ALA	54.5	17.7	178.7
288	GLN	57.7	28.1	177.6
289	SER	59.8	62.8	175.1
290	LEU	55.6	42.3	177.1
291	ILE	63.2	35.8	174.7
292	PRO	64.2	30.8	177.8
293	ARG	56.6	29.1	178.0
294	PHE	59.6	38.4	176.5
295	ASP	56.8	39.9	178.3
296	ASN	55.3	38.1	177.3
297	LEU	57.6	41.0	178.3
298	LEU	57.4	40.1	179.4
299	SER	60.7	62.4	176.6
300	LYS	57.6	31.5	178.2

Table S2. Residue-specific dissociation constant (K_D) for GDP and GTP

		Presence of GDP		Presence of GTP	
#	Residue	K_D (mM)	*sdv*	K_D (mM)	*sdv*
1	MET				
2	PRO			4.9	0.3
3	HIS	31.2	3.7	10.3	1.0
4	THR	8.5	0.8	3.3	0.0
5	ASP	8.1	0.7	2.8	0.1
6	LYS	6.3	0.6	2.9	0.2
7	LYS	10.8	0.9	3.6	0.2
8	GLN	6.9	0.4	2.6	0.1
9	SER	64.8	9.4	6.3	0.6
10	GLY	19.2	3.8	6.8	0.9
11	LEU	25.9	3.4	8.0	0.3
12	ALA	36.3	5.1	6.0	0.3
13	ARG	19.7	4.8	4.6	0.4
14	LEU	22.6	3.5	7.3	0.5
15	LEU			11.8	0.6
16	GLY				
17	SER	28.6	10.4	7.3	1.3
18	ALA			8.2	0.6
19	SER				
20	ALA				
21	GLY				
22	ILE				
23	MET	16.5*	11.4	4.5*	0.8
24	GLU	27.3*	2.0	5.6*	1.1
25	ILE	10.7*	1.6	5.0*	0.8
26	ALA	11.9*	1.0	4.0*	0.9
27	VAL	16.1*	0.6	5.1*	0.3
28	PHE	16.9*	1.8	4.8*	0.7
29	HIS				
30	PRO	10.2*	1.2	2.6*	0.1
31	VAL	19.7	2.5	7.2	0.7
32	ASP	16.7	1.7	5.2	0.6
33	THR	35.5	3.1	8.7	0.3
34	ILE	52.7	5.0	18.1	0.7
35	SER	33.0	6.7	12.1	1.2
36	LYS	42.1	5.2	10.9	0.8
37	ARG	54.7	5.5	13.0	0.6
38	LEU	38.8	10.6	12.2	0.8
39	MET	40.4	5.1	11.2	0.6
40	SER	20.9	5.5	11.9	0.8
41	ASN	71.5	12.7	22.6	2.0
42	HIS	34.4	6.2	13.3	1.5
43	THR			10.0	0.6
44	LYS	64.4	11.0	12.0	0.8
45	ILE	57.5	10.0	10.5	0.7
46	THR			77.6	1.5
47	SER			5.5	1.3
48	GLY	30.8	3.9	14.1	1.1
49	GLN	20.6	3.6	11.6	1.6

50	GLU	12.5	3.7	17.5	2.0
51	LEU	31.8	2.6	10.9	2.2
52	ASN	79.2	10.2	12.9	1.1
53	ARG	37.2	6.0	21.3	2.1
54	VAL	14.4	2.9	11.7	2.1
55	ILE				
56	PHE			12.9	5.1
57	ARG	183.0	12.9	24.4	1.5
58	ASP	46.4	26.3	13.9	2.1
59	HIS	63.8	11.0	12.8	0.9
60	PHE	72.6	13.5	15.4	1.1
61	SER			15.7	0.5
62	GLU				
63	PRO				
64	LEU				
65	GLY				
66	LYS	71.6	14.2	24.5	3.6
67	ARG				
68	LEU				
69	PHE	24.0	3.9		
70	THR			4.0	1.3
71	LEU	12.8	3.4	8.0	2.5
72	PHE				
73	PRO	12.0	0.9	6.8	0.3
74	GLY	18.3	1.8	6.5	0.3
75	LEU	23.9	4.6	7.6	1.1
76	GLY	31.4	3.6	7.1	0.8
77	TYR	9.7	0.7	4.0	0.6
78	ALA	22.4	4.9	7.2	0.7
79	ALA	24.1	2.4	7.9	0.3
80	SER	17.4	3.1	8.8	0.5
81	TYR	56.4	3.9	9.5	1.4
82	LYS	18.6	4.5	6.0	2.0
83	VAL	14.5	1.5	8.3	0.2
84	LEU	15.7*	1.4	7.5*	0.3
85	GLN	16.0*	2.6	7.8*	0.5
86	ARG	15.4*	1.8	5.8*	0.2
87	VAL	15.0*	2.6	6.4*	0.3
88	TYR	7.2*	1.6	5.0*	0.7
89	LYS	24.3*	2.3	6.5*	0.3
90	TYR	19.1*	2.0	6.5*	0.5
91	GLY	15.9*	1.5	6.1*	0.2
92	GLY	22.0*	2.9	6.5*	0.3
93	GLN	31.0*	4.2	6.7*	1.2
94	PRO	30.0	3.0	9.2	0.5
95	PHE	23.0	2.7	9.8	2.0
96	ALA	37.5	4.7	4.5	0.5
97	ASN	35.3	8.6	9.1	1.1
98	GLU	37.4	5.5	12.4	0.7
99	PHE	39.1	3.0	11.9	0.5
100	LEU	25.8	7.3	7.4	2.0
101	ASN	34.3	2.7	9.9	0.9
102	LYS	40.7	6.1	9.3	0.4

103	HIS	32.5	3.9	6.5	0.9
104	TYR	30.6	5.9	9.9	2.1
105	LYS	47.6	5.5	12.4	0.5
106	LYS	41.2	9.2	10.7	0.9
107	ASP	25.5	9.2	10.3	0.7
108	PHE	13.1	2.9	11.2	0.7
109	ASP	10.0	2.9	4.2	0.6
110	ASN	45.1	16.7	9.7	0.5
111	LEU	25.0	3.2	16.9	1.4
112	PHE			29.3	3.5
113	GLY	29.2	3.7	10.9	1.1
114	GLU	37.2	5.1	13.5	1.0
115	LYS	36.3	5.1	23.2	1.9
116	THR	31.7	4.2	7.0	0.3
117	GLY	31.9	5.1	7.0	0.3
118	LYS	36.4	7.4	6.3	0.5
119	ALA	10.2	2.2	8.6	1.9
120	MET			21.6	0.7
121	ARG			16.0	2.1
122	SER	12.6	7.6	6.0	1.4
123	ALA	7.5	1.5	10.0	1.9
124	ALA			16.9	1.2
125	ALA			10.8	2.5
126	GLY	35.5	5.1	11.9	1.0
127	SER				
128	LEU	19.4*	3.1	12.3*	2.5
129	ILE	46.9*	4.8	11.8*	3.1
130	GLY	49.2*	5.1	14.3*	2.4
131	ILE				
132	GLY	10.8*	2.1	8.1*	1.1
133	GLU			6.4*	0.8
134	ILE	20.4*	4.0	7.0*	3.7
135	VAL				
136	LEU			4.1	1.0
137	LEU				
138	PRO				
139	LEU				
140	ASP	47.2	4.3	25.0	5.0
141	VAL	18.5	3.4	4.6	0.8
142	LEU	48.1	5.1	12.0	0.3
143	LYS	32.3	7.6	9.3	1.4
144	ILE	34.1	4.9	8.4	0.4
145	LYS	41.7	4.7	9.6	0.6
146	ARG				
147	GLN				
148	THR				
149	ASN				
150	PRO	57.8	9.8	8.7	0.8
151	GLU	30.0	2.4	7.7	0.6
152	SER			12.3	0.6
153	PHE	45.1	2.8	2.5	0.7
154	LYS	18.9	4.2	2.3	0.5
155	GLY	25.1	2.5	6.7	0.3

156	ARG	35.0	4.5	6.6	0.4
157	GLY			5.8	0.7
158	PHE	37.0	4.5	4.8	0.4
159	ILE	39.8	5.4	7.4	1.2
160	LYS			4.3	0.7
161	ILE	48.0	3.7	8.4	0.5
162	LEU	39.8	13.0	6.4	0.4
163	ARG	51.5	8.6	14.5	0.7
164	ASP	51.7	11.9	11.5	1.5
165	GLU	54.0	15.7	10.9	3.0
166	GLY	29.2	7.4	9.8	1.1
167	LEU	54.1	10.7	10.3	0.6
168	PHE	23.5	3.0	10.3	0.9
169	ASN	29.1	7.2	11.7	1.1
170	LEU	54.6	5.5	19.8	1.9
171	TYR	46.8	5.8	18.1	1.1
172	ARG				
173	GLY	56.2	7.4	7.8	0.8
174	TRP				
175	GLY				
176	TRP	12.4*	2.0	5.1*	2.0
177	THR	29.2*	4.5	7.4*	0.7
178	ALA	28.7*	12.1	5.5*	0.9
179	ALA	14.0*	2.7	6.1*	1.7
180	ARG				
181	ASN	27.9*	1.9	1.6*	0.7
182	ALA	40.8*	3.8	1.9*	0.6
183	PRO				
184	GLY	11.9*	1.6	3.4*	0.6
185	SER	47.2*	5.4	4.0*	0.5
186	PHE	6.0*	0.5	3.0*	0.6
187	ALA	7.4*	0.9	3.4	0.9
188	LEU			3.1	0.5
189	PHE				
190	GLY				
191	GLY				
192	ASN			12.7	1.0
193	ALA				
194	PHE				
195	ALA	44.7	14.7	15.6	1.8
196	LYS				
197	GLU				
198	TYR				
199	ILE			19.6	2.1
200	LEU			5.7	1.4
201	GLY				
202	LEU			23.0	1.5
203	LYS			11.4	4.2
204	ASP			5.3	1.8
205	TYR			11.3	1.0
206	SER				
207	GLN				
208	ALA				

209	THR				
210	TRP				
211	SER				
212	GLN			3.5	0.3
213	ASN				
214	PHE				
215	ILE				
216	SER				
217	SER				
218	ILE				
219	VAL				
220	GLY				
221	ALA				
222	CYS				
223	SER				
224	SER				
225	LEU				
226	ILE				
227	VAL				
228	SER			2.7*	0.8
229	ALA			10.8*	2.6
230	PRO			6.5*	0.3
231	LEU	41.2*	5.7	13.4*	3.1
232	ASP	139.0	10.2	60.7	0.8
233	VAL	180.0	20.4	38.1	8.8
234	ILE	54.0	16.4	15.9	3.4
235	LYS	120.0	16.0	40.5	3.1
236	THR	112.0	12.2	36.1	2.0
237	ARG	198.0	25.8	67.9	6.0
238	ILE	146.0	29.9	36.6	3.3
239	GLN	142.0	18.2	50.5	10.3
240	ASN	603.0	30.1	20.2	3.9
241	ARG			40.5	6.4
242	ASN			13.0	1.5
243	PHE				
244	ASP				
245	ASN				
246	PRO				
247	GLU				
248	SER				
249	GLY				
250	LEU	24.8	5.1	57.9	1.9
251	ARG				
252	ILE				
253	VAL				
254	LYS	8.8	31.2	11.9	2.6
255	ASN	39.0	3.4	11.2	0.8
256	THR	33.6	2.7	11.5	0.5
257	LEU	59.7	9.6	15.7	0.7
258	LYS	80.2	16.8	9.7	1.5
259	ASN			13.3	0.9
260	GLU	99.1	28.9	15.8	2.2
261	GLY	54.0	11.6	14.2	0.9

262	VAL	55.2	8.6	18.5	3.1
263	THR	48.3	7.1	19.9	1.5
264	ALA	66.1	10.6	20.8	2.8
265	PHE	46.3	9.4	40.6	1.7
266	PHE	48.5	13.8	32.5	1.4
267	LYS	67.9	6.6	32.9	1.5
268	GLY	91.9	12.0	18.0	2.0
269	LEU	81.2	6.0	26.6	1.8
270	THR				
271	PRO	40.0	6.3	16.7	0.8
272	LYS	68.8	8.3	14.5	1.0
273	LEU		3.4	8.8	1.2
274	LEU	34.2	7.8	10.4	4.3
275	THR				
276	THR	51.7*	5.4	7.7*	0.6
277	GLY			3.2*	
278	PRO				
279	LYS	24.8*	1.9	20.1*	1.7
280	LEU			8.9*	1.8
281	VAL			2.5*	2.4
282	PHE	27.4*	2.3	6.1*	0.0
283	SER	39.0	3.6	7.8	0.5
284	PHE	13.2	3.8	8.9	2.0
285	ALA			11.0	0.6
286	LEU			5.3	0.4
287	ALA				
288	GLN	29.1	4.1	9.3	3.6
289	SER				
290	LEU			5.0	0.9
291	ILE			7.6	0.5
292	PRO				
293	ARG	8.9	2.1	3.2	1.1
294	PHE	9.9	1.0	6.2	0.3
295	ASP	28.0	3.6	11.0	0.3
296	ASN	14.9	2.2	7.8	0.7
297	LEU	15.3	1.9	5.1	0.3
298	LEU	17.5	3.8	6.1	0.4
299	SER	16.0	2.7	5.9	0.4
300	LYS	13.6	1.5	5.2	0.2

Table S3. Experimental internuclear RDCs couplings of GGC in presence and absence of GTP

		Absence of GTP			Presence of GTP		
#	Residue	$^1D_{NH}$ (Hz)	$^1D_{C'C\alpha}$ (Hz)	$^1D_{NC'}$ (Hz)	$^1D_{NH}$ (Hz)	$^1D_{C'C\alpha}$ (Hz)	$^1D_{NC'}$ (Hz)
1	MET						
2	PRO						
3	HIS						
4	THR		-1.20			-0.88	
5	ASP	5.2	3.42	-2.32	3.1	1.98	-1.5
6	LYS	-22.3		0.82	-13.0	-2.72	0.56
7	LYS	0.2	-3.55		-1.0	-7.21	2.48
8	GLN	4.2	1.42	-0.78	14.2	1.19	-0.8
9	SER	42.6	-3.81	-2.47	21.1		-1.31
10	GLY			1.06	16.9	-5.36	1.6
11	LEU	2.2		0.97	10.0	3.11	0.91
12	ALA				-16.8	2.99	-2.24
13	ARG	6.7		0.29	7.7	-2.29	0.25
14	LEU		-0.59		12.4	-0.07	0.52
15	LEU	-5.9		2.16	-15.0	2.32	2.95
16	GLY	-6.0			-10.9	1.84	-3.03
17	SER	12.4			8.1		0.21
18	ALA				2.5	1.19	0.78
19	SER	-28.1		-0.26	-25.3	4.56	-0.34
20	ALA	-16.2	-2.86	-1.56	-17.3	-4.30	-1.04
21	GLY	13.7		1.98	2.3	2.10	1.73
22	ILE						
23	MET		-0.44				-0.47
24	GLU	1.8		-0.07			
25	ILE	6.3	-3.60			-0.55	
26	ALA		2.81	0.21		1.47	0.51
27	VAL	-26.2	-3.29	-0.11	-19.1	-2.86	0.5
28	PHE	5.0	-3.42	0.99	-3.3	-2.89	1.13
29	HIS	-28.3			-17.7		
30	PRO		-2.00			-0.44	
31	VAL	-6.7	0.00	-0.04	-15.4		0.31
32	ASP	-23.3	-0.85	2.74	-10.7	0.66	1.7
33	THR	-26.4		-0.91	-16.8	2.26	-0.44
34	ILE	-22.3	-2.25	0.85	-13.7	-1.85	0.31
35	SER	-19.6	-0.68	-0.12	-6.2	-1.58	0.64
36	LYS		0.16	1.32	-9.9	0.14	1.1
37	ARG	-23.3	-0.80	1.60	-15.3	1.61	0
38	LEU	-13.4	-0.84	-0.48	-6.5	-1.25	-0.12
39	MET	-11.3	-0.73	1.75	0.7	-1.57	1.31
40	SER	-6.6	1.63	-0.39	-3.4	1.17	-0.04
41	ASN	0.1		-0.17	0.2		-0.54
42	HIS		1.45				
43	THR	1.5	2.06	-0.17		1.44	
44	LYS	0.1	-0.13	0.53	-0.2	-0.52	0.51
45	ILE	5.3	2.05	-0.53	3.8	2.00	-0.64
46	THR	-2.4	0.26	0.34	-0.5	-0.20	0.34
47	SER	-0.1	0.56	0.23	1.1	0.34	-0.32
48	GLY	-1.9	1.60	0.01	-0.6	1.30	-0.16

49	GLN	-1.1	-0.34	-0.17	0.3	-0.29	-0.35
50	GLU	2.2	-0.49	0.16	2.6	-1.30	0.36
51	LEU	3.9	-2.28	0.34	-0.9	0.79	0.27
52	ASN	1.3	3.26	-0.04	-4.0	-0.21	-0.01
53	ARG	-1.1	2.95	-0.65	-1.5	-0.03	-0.68
54	VAL	0.8		0.39	1.0		0.36
55	ILE						
56	PHE		2.06			0.98	
57	ARG	-1.2	0.57	-0.02	0.1	0.31	-0.21
58	ASP	-2.4		0.20	-1.5	0.00	0.17
59	HIS	-3.9	0.26		-1.2	-3.13	0.03
60	PHE	0.2	0.11	-0.66		0.20	-0.38
61	SER	-9.6		0.20	-0.7		0.52
62	GLU	-5.8		-0.06			
63	PRO						
64	LEU						
65	GLY	6.5			-4.3		
66	LYS	-2.7		0.78	-9.5		1.19
67	ARG	-8.1		-0.59	-8.1		-1.26
68	LEU	1.2		2.19	-0.5	-2.17	1.28
69	PHE	6.9		0.17	-0.3		-0.03
70	THR	-25.1	1.25		-14.5	1.01	0.07
71	LEU	-4.3	-1.70	-0.80	-3.6	-1.45	0.25
72	PHE	3.9		0.84	0.3		0.53
73	PRO		-2.23			-0.55	
74	GLY	-0.9	1.84	1.46	-0.7	1.93	0.73
75	LEU	-3.1			-5.8	1.50	-1.64
76	GLY	13.0			7.4		0.12
77	TYR		-1.11			-3.09	
78	ALA	1.3		-0.64	3.4		-0.61
79	ALA	21.5			17.3		1.69
80	SER		3.99		20.7	0.73	
81	TYR	-2.3	0.44	1.30	-5.3		0.81
82	LYS	-6.4		0.17			
83	VAL				20.6		-1.3
84	LEU						1.29
85	GLN				17.5		
86	ARG				20.1		1.9
87	VAL				21.9		
88	TYR						
89	LYS						
90	TYR						
91	GLY		6.31		16.5	1.72	
92	GLY	-12.9	0.39	-2.18	-7.0	0.20	-1.02
93	GLN	1.5		-0.35	-6.8		0.23
94	PRO						
95	PHE	-10.1		0.57	-8.4		0.84
96	ALA		-1.59			0.50	-0.22
97	ASN	-24.0		0.30	-10.2	0.33	0.44
98	GLU	-6.7	-0.65	0.94	-11.1		-0.09
99	PHE	-8.5	-0.28	1.95			
100	LEU	-9.2		-0.53			
101	ASN	-6.0	2.62	0.20			

102	LYS	2.8		-0.64	-3.7		-0.13
103	HIS	-8.8				0.08	
104	TYR	0.7	0.13	0.16	-1.3	-0.14	-0.46
105	LYS	-8.5	2.60	-0.02	-5.0		-0.52
106	LYS	8.4	-0.42	0.29		-0.57	
107	ASP	-5.1	-0.25	0.47	2.5	-0.43	0.31
108	PHE	-0.5	1.06	0.84	-1.2	0.03	1.07
109	ASP	-6.5	0.64	-1.06	-2.6	1.35	-0.88
110	ASN	-0.8	-0.46	0.68	-0.9	-1.74	0.52
111	LEU	-0.8	1.97	-0.10	0.9	3.03	-0.2
112	PHE	1.9	-0.59	-0.03	2.9	-0.60	0.18
113	GLY	3.4	1.06	-0.71	3.2	1.13	-0.83
114	GLU	0.8	1.88	-0.71	-0.9	0.35	-0.64
115	LYS	5.2	0.04	0.64	4.3	-0.85	0.3
116	THR	10.7	1.04	-0.57	7.2	0.52	-0.54
117	GLY	2.6	1.84	0.60	1.3	1.49	0.35
118	LYS	0.8		-1.64	-0.1		-1.14
119	ALA	8.0		0.85	6.2		0.34
120	MET	5.2	2.04	-0.01	1.9	1.29	0.22
121	ARG	2.7		-1.55	0.8		
122	SER	1.7	1.21	-0.80	3.6		0.05
123	ALA	6.8	-0.63	-0.32	3.8	-2.26	-0.25
124	ALA	1.9	1.86	0.89	0.0	1.37	0.54
125	ALA	-2.7	0.70	-0.33	-3.1	0.40	-1.16
126	GLY	1.7	-1.39	0.19	1.4	-1.73	0.07
127	SER	3.5	-0.12	0.05	1.5	-0.50	0.05
128	LEU	-7.3	0.63	0.50	-4.8	-0.26	0.29
129	ILE	-6.2	0.26	-0.53	10.5	0.10	1.31
130	GLY	-2.8	-0.35	0.36	-2.0	-0.54	0.21
131	ILE	-4.4	0.13	0.40	-1.0	0.10	0.54
132	GLY	-9.1	0.79	0.23	-6.7	0.74	0.05
133	GLU	-5.6	-0.47	0.09	-4.0	-0.15	-0.02
134	ILE	-0.9	3.81	0.56	-2.3		0.52
135	VAL	-9.2			-7.2		
136	LEU		1.42			-0.80	
137	LEU	-2.2		-0.13	-2.9		-0.17
138	PRO						
139	LEU	-5.2	0.94			0.97	
140	ASP	2.7		-0.96	-2.3	1.43	-0.04
141	VAL		0.43		-4.6	-0.23	0.65
142	LEU	-0.8	0.67	-0.02	-1.6		0
143	LYS	-2.3	1.08	0.18			
144	ILE	-2.3	0.13	-0.38	-2.2		-0.18
145	LYS	-0.7		-0.13	-0.7		
146	ARG						
147	GLN						
148	THR						
149	ASN						
150	PRO		2.44			0.84	
151	GLU	0.0	0.26	-0.72	-0.4	0.41	-0.3
152	SER	0.5	1.16	-0.16	0.9	-0.12	0.1
153	PHE	-1.0	-0.11		-1.6		
154	LYS	2.7	1.73	-0.74	2.7	1.08	

155	GLY	0.0	0.19	0.34		0.01	0.08
156	ARG	1.6	1.05	-0.64	-0.8	0.65	-0.39
157	GLY	-1.0	2.08	0.58	-0.7		0.38
158	PHE	4.6		-0.46	5.2	-0.76	-0.07
159	ILE	-1.6		-0.45	2.0		-0.53
160	LYS	1.3	1.39	-0.36	1.6	0.24	-0.41
161	ILE	9.5		-0.40	5.1		-0.54
162	LEU	-1.1			3.2		0.37
163	ARG						
164	ASP						
165	GLU						
166	GLY	-9.3	3.63	0.73		-3.43	
167	LEU	0.4		1.21	-24.3		1.8
168	PHE	-21.7			-3.3	0.79	-1.04
169	ASN	0.4	2.40	-0.17	0.2	-0.66	0.34
170	LEU	-1.5	0.57	-0.26	0.9	-2.28	-0.63
171	TYR	-2.3	-1.04	0.47	0.2	1.42	0.61
172	ARG	-7.6	0.54	-0.61	-1.0	1.53	-0.72
173	GLY	4.2	-3.14	0.48	2.6	-0.88	0.13
174	TRP	2.1	2.59	-0.38	2.4	0.98	0.03
175	GLY	-0.3	0.13	0.08	1.3	-0.17	0.14
176	TRP	0.7	-0.75	-0.03	0.5	0.06	0
177	THR	-2.8	-1.18	0.25	-3.7	1.12	0.04
178	ALA	-1.5	-0.62	-0.15	-1.8		0.04
179	ALA	-7.1			-4.9		
180	ARG						
181	ASN						
182	ALA						
183	PRO		0.89			0.49	
184	GLY	-3.6	0.50	0.10	-2.3	1.06	-0.07
185	SER	-1.1	-0.21	0.16	-0.4	-0.02	-0.06
186	PHE	-2.5	0.20	0.39	-1.7	0.19	0.25
187	ALA	-3.4	0.10	-0.12	-2.9	-0.26	-0.1
188	LEU	-5.6	-0.24	0.44	-2.1	-0.05	0.21
189	PHE	-0.6	0.88	-0.01	-0.5	0.34	0.02
190	GLY	-3.2	0.25	0.01	-1.6	0.16	0.06
191	GLY	0.8	0.04	0.07	0.5	0.10	0.04
192	ASN	-1.6	0.24	-0.14	-1.4	0.19	-0.14
193	ALA	-0.1	-0.64	0.33	-1.2	-1.94	0.16
194	PHE	-3.5	1.00	0.48	-2.4	0.08	1.5
195	ALA	-0.2		0.06	-2.0	-1.11	0.2
196	LYS		0.49		0.0	0.21	-0.06
197	GLU	-1.4	-0.43	0.37	-0.8	-1.22	0.23
198	TYR	-1.3	0.29	0.09	-1.0	0.22	-0.01
199	ILE	-1.1		-0.28	1.1		0.32
200	LEU		-0.19			0.38	
201	GLY	1.3	0.32	-0.89	-0.2	0.31	-0.54
202	LEU	1.4	-0.12	0.41	-0.4	0.52	0.27
203	LYS	-2.6	1.78	-0.06	-1.0	1.82	-0.47
204	ASP	0.2	0.89	0.05	-2.0	0.28	0.11
205	TYR	-0.9	0.39	-0.39	-0.3	0.66	0
206	SER	1.8	-0.51	-0.34	0.8	0.28	-0.14
207	GLN	2.2			-1.3		

208	ALA						
209	THR						
210	TRP						
211	SER						
212	GLN		0.83			1.70	
213	ASN	18.0		-0.80	6.0		-0.12
214	PHE	24.5	0.84	-1.04		0.57	-0.3
215	ILE	-5.2		-0.87	0.2		-0.37
216	SER	8.5	0.56		6.7		-0.37
217	SER	28.1		1.23			
218	ILE	6.7			4.5	-0.95	-0.54
219	VAL	5.8	-3.71	-0.49	9.1	0.05	-0.62
220	GLY	12.6	0.29	-1.41	9.8	0.18	-0.15
221	ALA	19.6		0.73	9.3		-0.29
222	CYS	6.1			5.1	0.40	-0.22
223	SER	16.8	2.33		6.8	0.85	-0.49
224	SER	13.3	-1.41	-1.26	11.1	0.03	-0.39
225	LEU	6.0	-1.04	-0.24	7.9	0.35	-0.68
226	ILE	-1.3	-3.40	-1.23	5.4		-0.39
227	VAL	6.2	-0.45		3.9	-0.19	
228	SER	4.1	1.13	-0.01	2.7	0.56	-0.04
229	ALA	0.3		-0.70	3.3		-0.52
230	PRO		-7.74				
231	LEU	-26.3	-2.88		-2.9		
232	ASP	3.8	-1.08		-0.4	-1.27	
233	VAL	10.3	-1.81	-0.66	7.0	-1.48	-0.39
234	ILE	3.8	0.24	1.57	0.2	0.00	1.16
235	LYS	-7.2	1.08	-1.13	-5.6	2.96	-1.18
236	THR	0.3	-1.39	-0.95	-3.0	-1.39	-0.44
237	ARG	22.6	-2.07	0.42	14.5	0.16	0.57
238	ILE	-3.3	3.13	-0.24	-2.2	1.76	-0.32
239	GLN	-2.9	0.89	-0.35	-4.0	1.78	-0.3
240	ASN	3.6	-1.00	-0.91	1.2	-0.87	-0.51
241	ARG	9.0	1.13	0.41	1.0	0.53	0.53
242	ASN	-6.1	0.91	-0.30	-4.7	0.52	-0.24
243	PHE	-1.8	0.87	-0.35	-2.9	0.29	-0.22
244	ASP	-2.1	1.90	-0.15	-3.7	0.55	-0.07
245	ASN	-6.1			1.7		
246	PRO						
247	GLU						
248	SER						
249	GLY		1.32			0.99	
250	LEU	2.4	-1.81	-0.07	3.4	-1.92	-0.23
251	ARG	16.6	-0.45	0.85	12.9	-0.32	0.8
252	ILE	-6.9	2.27	-1.46	-5.5	2.34	-0.8
253	VAL	1.2	-0.99	-0.02	0.3	-1.74	0.21
254	LYS	0.1	-0.59	0.36	6.5	-0.53	-0.96
255	ASN	4.5	2.05	1.39	2.8	-0.02	1.18
256	THR	-16.3	0.67	-1.88	-2.3	1.39	-1.79
257	LEU	4.9	-0.85	0.91	2.9	-2.92	0.18
258	LYS	20.6	0.25	0.08	3.7	0.17	0.38
259	ASN	-6.7	0.67	0.29	-2.0	0.80	0.05
260	GLU	-5.2	2.12	0.60	3.9	1.30	-0.56

261	GLY	7.2	-0.81	-0.59	4.8	-0.84	-0.58
262	VAL	1.2	-0.59	0.40	4.4	0.45	0
263	THR	4.5	1.03	-1.15	5.8	0.52	-0.36
264	ALA	6.8	-0.72	0.45	7.1	-1.16	0.41
265	PHE	7.5		-1.29	4.9		-1.29
266	PHE		-1.56			-1.59	
267	LYS	4.5	1.90	-1.40	6.6	1.19	-1.04
268	GLY	6.3	-0.74	0.23	3.9	-0.55	0.33
269	LEU	11.3	1.88	-0.86	6.8	1.70	-0.71
270	THR	-3.5		0.28	-0.6		0.31
271	PRO		0.57			0.63	
272	LYS	8.5	-0.46	-0.06	5.8	-1.57	0.19
273	LEU	15.0	0.78	0.08	6.0	0.37	0.22
274	LEU	5.2		-0.46	-1.6		0.06
275	THR		0.53		4.0	0.72	
276	THR	2.1	-0.98	0.71	2.3	-1.15	0.28
277	GLY	-2.7		0.31	-0.5		0.3
278	PRO						
279	LYS					-0.07	
280	LEU	-3.3		1.26	-1.0		0.39
281	VAL	-9.6		0.72	-8.0		-0.02
282	PHE		3.96			1.30	
283	SER	-8.7	-0.63	-0.86	-5.5	-1.21	-0.59
284	PHE	-5.5		1.40	-2.9	-2.20	0.83
285	ALA	-5.3	0.92		-11.6	0.29	1.21
286	LEU	-27.4	0.97	-0.60	-18.4	-0.24	-0.08
287	ALA	-14.5	-4.19	0.76	-10.9	-2.86	0.38
288	GLN	-10.8	-0.98	1.93	-7.4	-0.85	1.54
289	SER	-31.9	0.39	1.13	-16.0	1.35	0.68
290	LEU	-22.2	-0.31	-0.30	-16.3	0.15	-0.11
291	ILE	2.7		1.83	-0.1		0.92
292	PRO					3.09	
293	ARG				-14.6	2.65	-0.55
294	PHE	3.9		-0.91	0.0	-0.65	-0.66
295	ASP	20.0		1.67	7.5	0.04	0.96
296	ASN				-0.5	3.67	-0.55
297	LEU	-11.7	3.59		-9.7	2.49	-3.13
298	LEU	17.5	-6.35	2.31	8.1		1.61
299	SER	19.9		-0.12	9.6	1.88	-0.1
300	LYS	-28.3		0.81	-13.2		0.98

Table S4. Example of RDC-based Molecular Fragment Analysis [a]

#	*sequence*	Q_{free}[b]	*s.d.*	Da[c]	*s.d.*	Rh[d]	*s.d.*	N[e]	GDO[f] [x10^{-3}]	*s.d.*	rmsd[g]
12	SGL**A**RLL	0.19	0.01	20.5	2.0	0.16	0.07	20	2.21	0.23	0.172
13	GLA**R**LLG	0.17	0.01	19.1	0.9	0.16	0.04	21	2.06	0.16	0.139
14	LAR**L**LGS	0.19	0.01	19.3	1.3	0.19	0.05	20	2.09	0.30	0.203
15	ARL**L**GSA	0.20	0.01	19.3	1.5	0.20	0.06	20	2.09	0.21	0.220
16	RLL**G**SAS	0.22	0.00	16.8	0.6	0.42	0.07	20	1.91	0.13	0.162
17	LLG**S**ASA	0.17	0.01	19.4	1.8	0.51	0.08	20	2.26	0.16	0.188
18	LGS**A**SAG	0.18	0.01	20.3	0.9	0.26	0.04	19	2.22	0.18	0.178
19	GSA**S**AGI	0.14	0.01	16.4	0.8	0.38	0.05	17	1.84	0.11	0.164
20	SAS**A**GIM	0.14	0.01	15.7	1.4	0.43	0.12	15	1.79	0.28	0.178
21	ASA**G**IME	0.10	0.01	18.3	1.7	0.22	0.12	13	1.99	0.47	0.208
22	SAG**I**MEI	0.05	0.01	17.4	1.4	0.34	0.12	11	1.93	0.13	0.189
23	AGI**M**EIA	0.06	0.01	18.2	2.2	0.25	0.13	10	1.99	0.11	0.184
24	GIM**E**IAV	0.05	0.01	14.4	4.4	0.15	0.08	10	1.56	0.12	0.204
25	IME**I**AVF	0.08	0.01	13.5	0.8	0.20	0.02	11	1.46	0.10	0.194
26	MEI**A**VFH	0.06	0.01	13.5	0.8	0.19	0.02	11	1.46	0.09	0.178
27	EIA**V**FHP	0.07	0.01	13.3	0.7	0.18	0.02	11	1.44	0.12	0.198
28	IAV**F**HPV	0.13	0.01	11.4	0.5	0.30	0.07	13	1.26	0.09	0.223
29	AVF**H**PVD	0.16	0.01	10.6	0.4	0.37	0.07	15	1.19	0.04	0.167
30	VFH**P**VDT	0.16	0.01	10.8	0.6	0.49	0.09	16	1.25	0.07	0.217
31	FHP**V**DTI	0.16	0.01	9.9	0.4	0.40	0.07	16	1.12	0.04	0.191
32	HPV**D**TIS	0.12	0.01	9.4	0.2	0.37	0.02	16	1.06	0.04	0.180
33	PVDT**I**SK	0.15	0.01	9.1	0.6	0.39	0.03	18	1.02	0.09	0.195
34	VDT**I**SKR	0.16	0.01	8.5	0.2	0.43	0.03	20	0.96	0.08	0.161
35	DTI**S**KRL	0.15	0.01	8.1	0.2	0.52	0.06	21	0.94	0.06	0.147
36	TIS**K**RLM	0.13	0.01	8.4	0.7	0.54	0.08	21	0.98	0.16	0.176
37	ISK**R**LMS	0.19	0.01	7.0	0.7	0.60	0.10	21	0.84	0.27	0.212

[a] Example of GDO values shown in Fig. S9b&c are shaded in grey. All the parameters are average of the 20 best fragment extract from SVD fit with PALES.
[b] Q_{free} is the free quality factor.
[c] Da is the magnitude of the alignment normalized to $^1D_{NH}$.
[d] Rh is rhombicity of the alignment tensor.
[e] N is the number of RDCs for the fragment.
[f] GDO is the general degree of order as defined by Equation 2.
[g] backbone root mean square deviation between the 20 best fragments.